A MODEL STUDY OF INTERANNUAL AND DECADAL VARIABILITY OF THE ARCTIC AND SUB-ARCTIC OCEANS

SARAH EMILY MAE LUNDRIGAN

A Model Study of Interannual and Decadal Variability of the Arctic and Sub-Arctic Oceans

by

© Sarah Emily Mae Lundrigan

A thesis submitted to the

School of Graduate Studies

in partial fulfilment of the

requirements for the degree of

Master of Science.

Department of Physics and Physical Oceanography

Memorial University of Newfoundland

August 2010

St. John's Newfoundland

Abstract

In this work I investigate the interannual and decadal variability in the properties and the transformations of the Atlantic Water (AW) mass using an Ocean General Circulation Model. A course resolution tri-polar grid coupled ocean/sea ice model (NEMO-OPA/ NEMO-LIM) is forced with atmospheric parameters from NCEP/NCAR reanalysis. The quality of the model is assessed through comparison with observations.

The model results show that there are in general two major processes that influenced the heat and salt balance of the Arctic and Sub-Arctic between 1985 and 2005. In the first decade of this period the volume flux of Atlantic Water into the Nordic Seas was not balanced by the outflow of Atlantic Water into the Arctic. This was a period of increase of the Atlantic Water volume and temperature in the Nordic Seas. Secondly, the Atlantic Water inflow into the Nordic Seas was warmer and saltier than normal between 1995 and 2005. THese two processes caused a rise in the model temperature of the Arctic and Sub-Arctic similar to observed warming trend in these regions.

Acknowledgements

I would like to convey thanks to MUN, CFCAS and NSERC for funding my research and I would like to thank the reviewers of this thesis for their time.

It is difficult to overstate my gratitude to my supervisor, Dr. Entcho Demirov. With his inspiration and his great ability to explain things clearly and simply to me he helped me to learn a great deal about oceanography and modelling. Throughout my thesis-writing he provided encouragement and sound advice. I would have been lost without him.

I would also like to thank my husband Adam, who helped with everything from writing Fortran Code, to editing my thesis, to helping me find time to relax. Without his encouragement and support I would not be where I am today.

Lastly, I wish to thank my parents, Kathleen and Michael Graham for their continuous support and understanding.

Contents

List of Figures

List of Tables

List of Acronyms

AWCT	Atlantic Water Core Temperature
AWL	Atlantic Water Layer
BWCT	Bottom Water Core Temperature
CAA	Canadian Arctic Archipelago
IPCC	International Panel on Climate Change
LH	Latent Heat
LIM	Louvain-la-Neuve sea ice model
MIW	Modified Icelandic Water
NAO	North Atlantic Oscillation
NAW	North Atlantic Water
NEMO	Nucleus for European Modelling of the Ocean
NSW	Nordic Sea Water
PSU	Practical Salinity Unit
PW	Polar Water
SH	Sensible Heat
SPG	Sub-Polar Gyre
SST	Sea Surface Temperature

Chapter 1

Introduction

The Arctic and Sub-Arctic oceans have an important impact on global climate. The sea ice in these oceans demonstrates strong seasonal and interannual variability. It impacts the global climate through the so called ice-albedo feedback. A loss of sea ice will decrease the albedo of the polar regions and so increase the global temperature. This increase in global temperature in turn decreases the sea ice concentration. This warming in the Arctic and Sub-Arctic would subsequently increase the temperature of the overflowing water from the Arctic to Sub-Polar region through the Denmark Strait. This is expected to affect the overturning circulation that occurs there, which may potentially impact the global circulation. Melting sea ice also results in a freshening of the surface which will strength the stratification in the Sub-Polar region and will therefore have an effect on the overturning circulation.

A significant decreasing trend, of $(2.6 \pm 0.6)\%$/decade [1], has been observed in the average sea ice extent since satellite observations began in 1978. A more startling trend is the decrease in minimum sea ice extent at the end of summer, which is

retreating by $(7.4 \pm 2.4)\%$/decade [1]. The Fourth Assessment Report of the IPCC states [1]:

> "on the basis of submarine sonar data and interpolation of the average sea ice thickness in the Arctic Basin from a variety of physically based sea ice models, it is very likely that the average sea ice thickness in the central Arctic has decreased by up to 1 m since the late 1980s."

A more precise estimate suggests that since 1978 the average rate of decrease in sea ice thickness is $(2.9 \pm 0.4)\%$/decade[2]. The decreasing trend in the summer minimum of the sea ice extent results in a decrease in the sea ice thickness. Less sea ice cover results in less ice that becomes thicker multi-year ice.

Observations also show that there was a significant increase in the sea surface temperature in the sub-polar ocean after 1995 [3] and an increase in the sub-surface temperature of the Irminger water off the west coast of Greenland [4] between 1991 and 2006. This warming off the coast of Greenland is causing a rapid acceleration in the flow of the outlet glaciers of the Greenland Ice Sheet. It is related to the changing atmospheric forcing. In particular some previous studies demonstrated that the North Atlantic Oscillation has an impact on the sea ice extent and inflow into the Nordic Seas [5, 6] and temperature and salinity of the sub-polar water in the North Atlantic [7].

The Arctic and Sub-Arctic region is important for the global climate. Previous model and data studies defined the major trends in the variability of these regions. However,still not much is known about the mechanisms of formation of this variability [8, 9, 10, 11, 12]. The present study is an attempt to identify the dominant patterns

and processes that influenced the changes in Arctic and Sub-Arctic oceans in the last 40 years.

1.1 Overview of Present Study

A global ocean model is used in this study to simulate the Arctic and Sub-Arctic Oceans for the period 1965-2005. An ocean model is used in this study because observations are sparse in the Arcitc region. The year round sea ice coverage and the extreme weather in the Arctic ocean makes it difficult to obtain uniform observations. There is often a seasonal bias in observations in polar regions because of the difficulty in deploying ships and crews in the winter months. First the model results are compared with observations in this region and the model skills are assessed. Then the interannual and decadal variability in the Arctic and Sub-Arctic Oceans is studied. The objectives of this study are to assess the role of recently observed atmospheric interannual and decadal variability in the Arctic and Sub-Arctic and evaluate the impact of this variability on the volume and heat transport in to Nordic Seas. More specifically in this study I address the following questions:

- What were the changes in the heat and volume fluxes in the Sub-polar and Sub-Arctic oceans from 1965 to 2000?
- How did these changes influence the heat balance of the Arctic and Sub-Arctic from 1965-2005?
- How are these changes related to the variability of the surface forcing?

The thesis is organized as follows: chapter 2 presents the background information of the Arctic and Sub-Arctic climate and interannual variability. Chapter 3 describes the model setup and model experiments. Chapter 4 uses the model results to demonstrate the climatic characteristics of the Arctic and Sub-Arctic Oceans. The variability and their mechanisms are discussed in chapter 5. Finally, conclusions are made in chapter 6. Chapter 7 presents some ideas about future extensions of the present study.

Chapter 2

Background

2.1 General Characteristics of the Arctic and Sub-Arctic Ocean

The Arctic Ocean and Nordic Seas are partially enclosed basins located at high latitudes in the Northern Hemisphere. The Arctic Ocean is located at the top of the world and it covers an area of 11.5 million km^2. Land surrounds it at latitudes of about 70 to 80^o north. The Nordic Sea is the region enclosed by Greenland to the west, Norway to the east, Iceland to the south and Spitsbergen to the north.

The fact that the Arctic Ocean and Nordic Seas are semi-enclosed means that they have a very large coastline to total volume ratio when compared with other oceans. This means that coastal runoff has a relatively large effect on the whole ocean [13, 14]. This is especially the case in the Arctic Ocean which drains some of the largest rivers in the world. The four major rivers that run into the Arctic Ocean

are the Ob, Yenisey, Lena, and Mackenzie. The total river run off into the Arctic Ocean is about 3300 km^3/yr [13]. There are no major rivesr that run into the Nordic Seas. The main source of freshening here is sea-ice melt and flow from the Arctic [15]. The extensive coastline also acts as a barrier for sea ice. The sea ice is moved by the wind which forces the ice against the shore. This leads to ice rafting on top of itself which leads to thicker ice packs, mostly along the northern edge of Canada.

The topography of the Arctic Ocean is formed by the progress of the plates drifting to the south. As seen in Fig. 2.1 there are two major deep basins that comprise the Arctic Ocean, the Canadian Basin with a maximum depth of $3500m$ and the Eurasian Basin with a maximum depth of $4000m$. The Eurasian basin is located north of Europe and Siberia and is surrounded by the Barents, Kara and Laptev seas. The Canadian Basin is located north of the Canadian Arctic Archipelago (CAA), Alaska and Eastern Siberia. These basins are separated by the Lomonosov Ridge with a maximum sill depth of about $1870m$ [16]. The Eurasian Basin is smaller and deeper than the Canadian Basin.

In this thesis 'polar region' refers to the Nordic Seas and the Arctic Ocean. Subpolar ocean refers to the part of the North Atlantic between 50 and 65°N.

The Nordic Seas refer to the Greenland and Norwegian Basins and the deeper waters in between.They are separated by the Mohn's Ridge which divides the deep waters into the two basins north to south. The average depth of these basins is about 1500m with a maximum depth of $3500m$ [17].

The Arctic Ocean is almost completely closed except for the connections through a few straits with the rest of the world. These straits are generally shallow and allow

just a restricted exchange of water masses. This is case for the Bering Strait, which is only $90km$ wide and $50m$ deep, the many arduous channels through the CAA, the Barents Sea and the Nares Strait.

The only strait that allows for transport of water below $250m$ is the Fram Strait. It is located between Greenland and Spitsbergen and is about $2600m$ deep for almost $250km$. This strait is the only place where surface, intermediate and deep water are freely transported in and out of the Arctic Ocean. The other flow routes from the Atlantic are blocked below $250m$ and the flow from the Pacific Ocean via the Bering Sea is blocked below $45m$. The water that enters the Arctic Ocean via the Fram Strait from the Atlantic Ocean must pass over the Greenland-Scotland Ridge and then through the Nordic Seas. The Greenland-Scotland Ridge is a ridge with a sill depth of $200 - 500m$ between Greenland and northern Scotland that passes through Iceland [18].

2.2 Atmospheric Climate

A major physical factor that defines the Arctic climate is the surface solar radiation. In the summer a relatively large amount of radiation penetrates through to the surface and in the winter the solar radiation is very little due to the Earth's tilt. Also, at high latitudes water has a fairly high albedo due to the sun's low height above the horizon. A large portion of solar radiation that does reach the Arctic Ocean surface is reflected away due to the high albedo of the sea ice and snow.

The climate of the polar region can be divided into two subtypes, maritime and

Figure 2.1: Topography and geographical names [19]

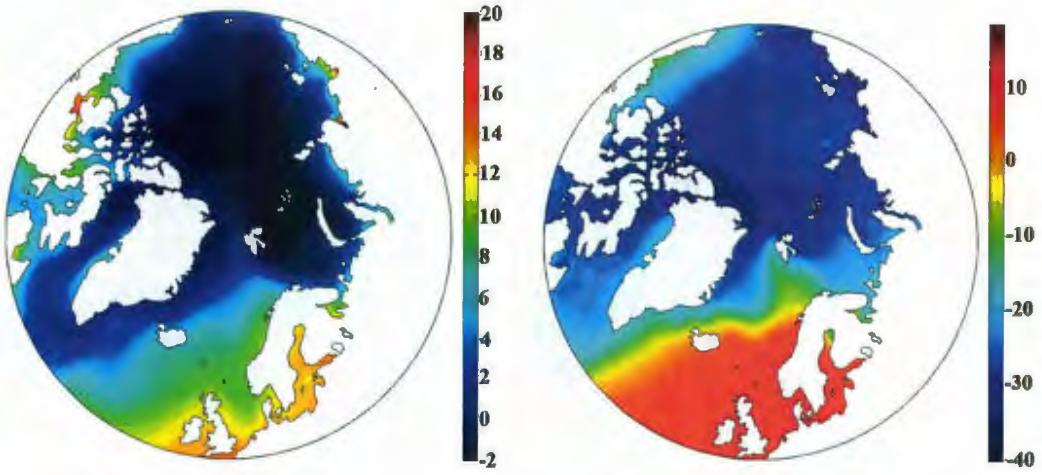

a July b January

Figure 2.2: Air Temperature in ^oC at 2m above the surface for (a) July and (b) January. [20]

continental. Maritime climate is the climate of Iceland, Norway, the adjacent part of Russia and near Alaska. The continental climate is the climate near eastern Alaska, the CAA and in the center of the Arctic Ocean. Areas with a maritime climate have moderate temperatures and stormy winters, while areas with a continental climates are cooler and are not as stormy as the maritime areas.

Maritime areas are mild with a mean temperature in the summer of 10°C and a mean temperature in the winter of −5°C (see Fig. 2.2) [19]. In continental areas the winters are much colder with a mean air temperature below −20°C over the CAA and Siberia and below −30°C over the central arctic. The summers in continental areas are only slightly cooler than the summers in maritime areas with an average temperatures of $5 - 10$°C over the CAA and Siberia and $0 - 2$°C over the central arctic [19].

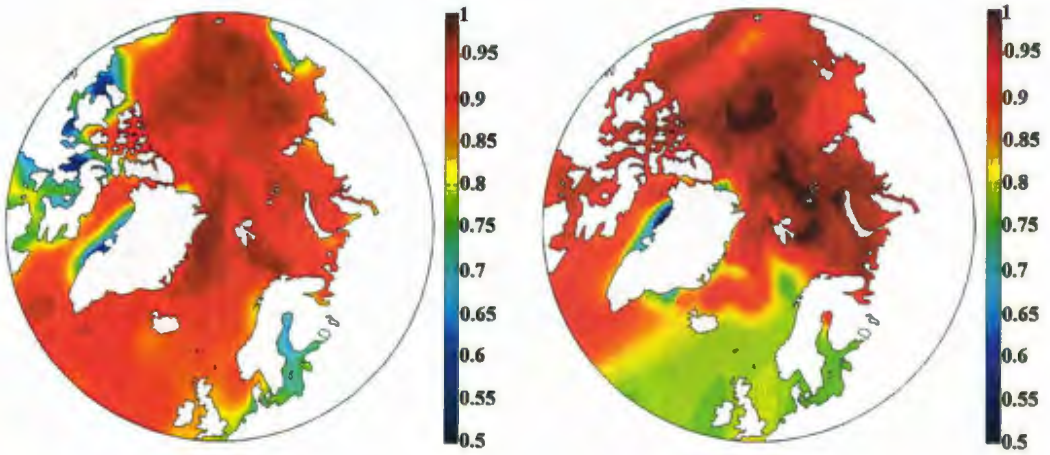

a July b January

Figure 2.3: Relative Humidity at 2m above the surface for (a) July and (b) January. [20]

The polar air mass is cold and has a low moisture content. Figures 2.2 and 2.3 show that the air mass over the central Arctic is colder and has a high relative humidity; where as the regions of maritime climate are warmer and have a lower relative humidity. The air masses over open water have a larger moisture content than over the sea ice but are warmer and therefore have a lower relative humidity. The lower moisture content over the sea ice is due to the blocking of evaporation from the ocean by the ice. A typical value of relative humidity at the surface in the Arctic is about 80 to 95% [21].

Stratus cloud cover is persistent and extensive over the polar region. Most of the clouds are formed in the summer and are a result of the transport of mild, humid air into the Arctic. The stratus cloud cover is about $70 - 90\%$ in the summer and decreases to $40 - 60\%$ in the winter [19]. Fog is another persistent feature of the

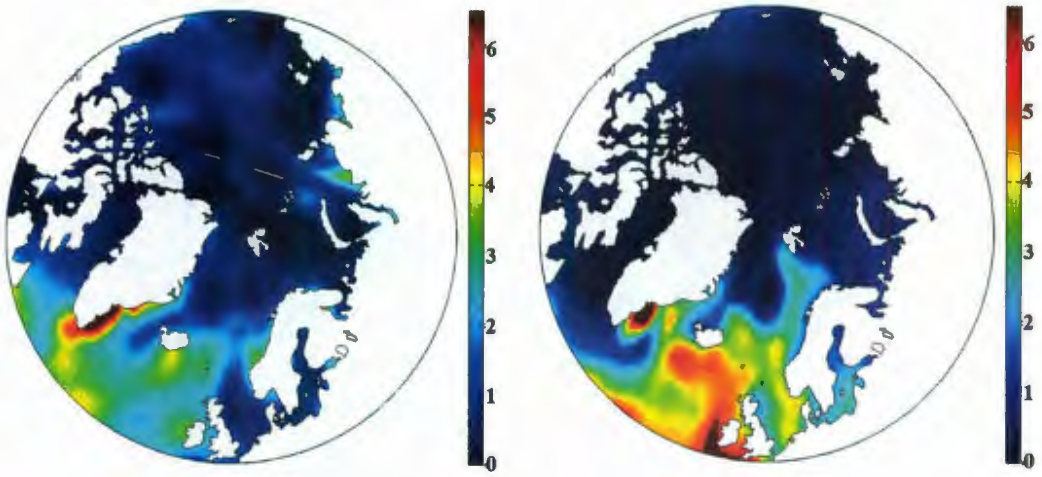

a July b January

Figure 2.4: Precipitation above the surface in $[kg/m^2/day]$ for (a) July and (b) January. [20]

region. The fog is a result of the movement of cold air over warm open water in some areas or wet air moving over cold ice in other areas. It is typical in some places to have more than 100 days of fog in a year [19].

The total annual precipitation in the polar region is usually less than $500mm/\text{year}$. It is higher in maritime and coastal areas and lower in the center of the ocean [19]. In the maritime and coastal areas, such as southern Iceland, and southern Alaska, the surface can receive more than $3000mm$ of precipitation in a year; whereas parts of the Arctic Ocean with a continental climate receive less than $150mm$ in a year[19] [22] . Due to the cold temperature of the Arctic the air masses are not able to hold as much water as the air at lower latitudes. Therefore even if the frequency of precipitation is high the intensity is low. This is also the reason for the smaller amount of total precipitation in the winter.

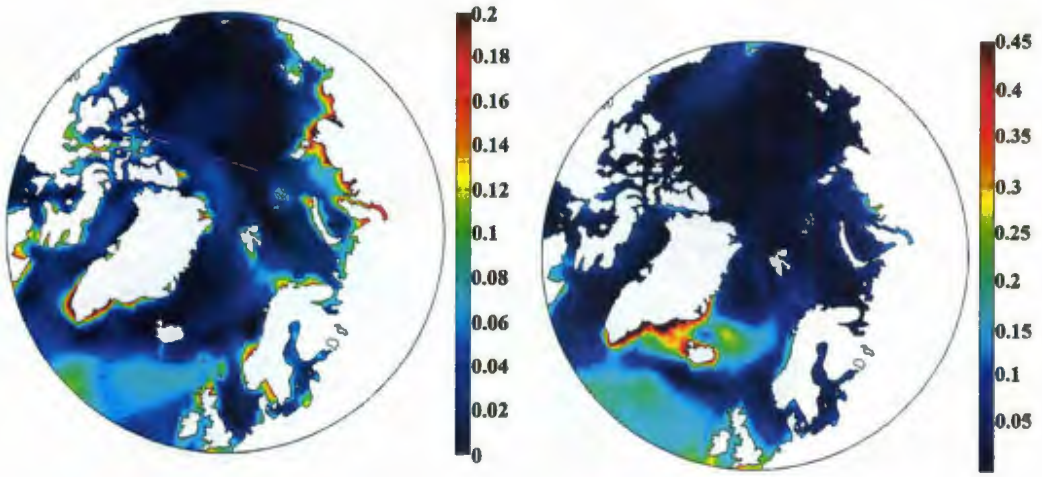

a July b January

Figure 2.5: Wind Stress in $[N/m^2]$ at the surface for (a) July and (b) January. [20]

The seasonal mean surface winds over the Arctic Ocean vary from about $5.1m/s$ in the summer to about $4.9m/s$ in the winter. The highest annual wind speeds are observed in the section of the Arctic Ocean adjacent to the Nordic Seas [23]. The speed of the surface winds over the Arctic Ocean are affected by normally stable stratification and the near-surface inversions. The inversions reduce the momentum flux between the stronger upper winds and the weaker near surface winds. Thus, the surface wind speeds in the winter are lower than the speeds in the summer because of the stronger and more frequent inversions in the winter [22]. The winter wind stresses are, however, higher due to increased drag over the sea ice (Fig. 2.5). Another important class of surface winds over the Arctic Ocean are the katabatic winds. They are a result of cold (dense) air that flows down slopes. This type of wind is common over the Greenland Ice-Sheet and along its edge where they often reach speeds of $100km/hr$ [22].

The large scale atmospheric circulation in the Arctic region is characterized by the Icelandic and Aleutian lows and the Siberian High. In the summer the atmospheric sea level pressure is characterized by relativity weak gradients in the polar and sub-polar regions with the sub-tropical highs in the Atlantic and Pacific Oceans (see Fig. 2.6).

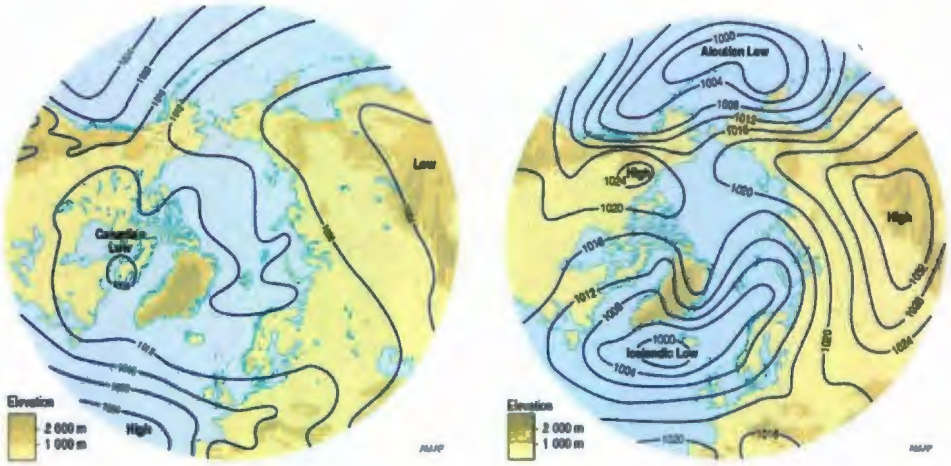

a July b January

Figure 2.6: Mean sea-level pressure (mb) in the Arctic for (a) July and (b) January. [19]

The general circulation is anticyclonic around the pole. Therefore, the prevailing winds are easterlies and north-easterlies and are know as the Polar Easterlies [19]. The Polar Easterlies do not form a global wind belt like the westerlies and trade winds. The easterlies occur on the northern side of the Icelandic low, located between Iceland and the southern tip of Greenland in the winter, and Aleutian low, located near the Aleutian Islands of Alaska [22]. The Aleutian low weakens and almost disappears in

the summer and the Icelandic low weakens and moves to southern Baffin Island in the summer. In the summer the large scale winds are more circular around the pole whereas in the winter there is a mean flow out of Eurasia in to the Arctic and out the Arctic and into North America [24].

A prominent pattern of the North Hemisphere atmospheric decadal variability is the North Atlantic Oscillation(NAO). It has a strong signature in the surface pressure. The NAO describes the co-variability in the sea-level pressure between the Azores High and the Icelandic Low. The NAO index is said to be positive when both are stronger than normal (see Fig. 2.7a). When both are weak the index is negative (see Fig. 2.7b). When the NAO index is positive the westerlies are stronger than usual. The years of a strong positive NAO index is associated with warmer, wetter winters in Eastern North America and Europe and colder, dryer winters in Greenland and south-eastern Europe. The NAO index was mostly negative in the 1960s, increasing between 1980 and the early 1990s and was mostly positive in the 1990s,(see Fig. 2.7c) [2]. This shift has been shown to affect the water masses of the North Atlantic and Sub-Polar Oceans [3, 27, 6]. The NAO is an important forcing for the North Atlantic. Interannual sea surface temperature anomalies are driven by local changes in the atmospheric heat flux. However, decadal anomalies are more influenced by changes in the large scale ocean circulation and therefore through changes in the surface forcing, such as the NAO [28]. The shift from mainly negative to mainly positive NAO also has the effect of increasing the amount of Atlantic water entering the Arctic Ocean, which will negatively affect sea ice extent [27].

There are other large scale patterns of variability in the Arctic region. The Arctic

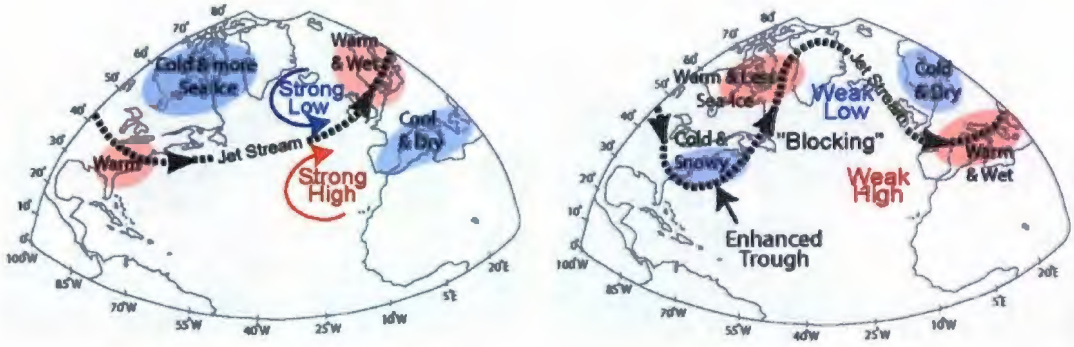

a Positive NAO

b Negative NAO

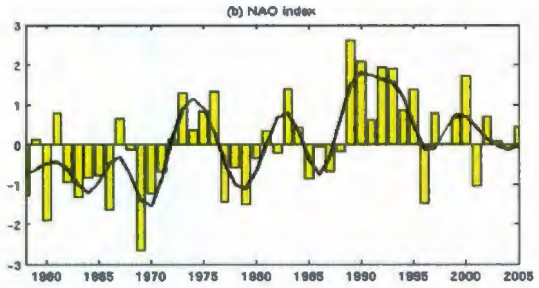

c NAO time series

Figure 2.7: Schematic of the NAO in (a) Positive and (b) Negative Phases. [25] (c) Time-series of NAO variability, data from J.W. Hurrell [26]

Oscillation is closely related to the NAO but is characterized by a sea level pressure anomaly in the Arctic and the opposite anomaly at $35 - 45°$N. The Arctic is experiencing linear climate change in almost all indicators while the Arctic Oscillation changes are more episodic. This is known as Overland and Wang's 'Arctic Paradox' [29]. The relation between any large scale atmospheric pattern and the climate is very complicated and needs to be studied very carefully.

Another pattern of large scale atmospheric variability is the Arctic Dipole Pattern (ADP). It is characterized by high pressure in the Arctic region of North America

and low pressure in the Eurasian region and is linked to drier winters in Northern Europe and colder winters in East Asia. The ADP allows more southern winds into the Arctic Ocean which results in more ice melting in this area [30, 31, 32].

There is much discussion into which of the NAO, the ADP and the Arctic Oscillation is the main driver of climate change in the Northern hemisphere [33, 34]. However, from Lohmann et. al. and Marsh et. al. [7, 3] it is known that the NAO is an important driver of the North Atlantic ocean climate, in particular the climate of the sub-polar region, and therefore a major influence on the waters that enter the Nordic Seas which is the main topic of this thesis.

2.3 Water masses and Circulation

The major water masses of Arctic Ocean are the Surface Arctic Water($0 - 200m$), Atlantic water ($200 - 900m$) and Bottom water($900m$-bottom). These layers are identifiable in most parts of the ocean, but they can vary regionally [35].

Surface Arctic Water is influenced by river runoff, ice melt, brine rejection, heat loss and absorption in open water and ice covered zones as well as inflow and mixing of the Atlantic and Pacific water. The Surface Arctic Water salinity is between 27 and 30 PSU near areas of freshwater influx such as a large river or the Bering Strait. It is between 33 and 34.5 PSU where the water is influenced by advection into the Arctic of Atlantic water. Below the top $30 - 50m$ temperature and salinity are more uniform horizontally. The temperature has a local maximum at $50 - 100m$ and then decreases to about $-1.5°C$ at $150m$ where it then increases to $0°C$ [35].

The Atlantic Water is beneath the Surface water and is located between 200 and $900m$. These depths contain the main thermocline. The temperature increases from the surface layer values, -1 to $0°C$, to about $0.5°C$ at about $250 - 500m$ depth depending on location. Below this the temperature decreases to negative values. The salinity increases below the surface until it reaches a nearly uniform salinity in the bottom of the layer with $34.9 - 35$ PSU in the Arctic Ocean and $34.5 - 34.6$ PSU in Baffin Bay. The warmest core of the Atlantic Water is found along the continental slope of the Eurasian Basin with temperatures between 1 and $1.5°C$ and the coldest is north of Ellesmere Island with a temperature of $0.38°C$ [35]. For the rest of the ocean the temperature of the core is about $0.5°C$.

Below the Atlantic Water is the Bottom Water. Less is known about this layer because of a limited amount of data. The bottom layer contains 60% of the water in the Arctic Ocean and its temperature everywhere is below $0°C$ [35]. The depth of a minimum temperature of -0.8 to $-0.9°C$ in the Eurasian Basin is $2500m$. The depth of a minimum temperature of -0.4 to $-0.5°C$ in the Canadian Basin is $2000m$. The salinities everywhere are 34.92 to 34.99 PSU [35]. The source for all of the bottom layer is the deep water that is formed in the Greenland-Norwegian Sea.

In the Greenland-Norwegian Seas the water masses are defined differently than in the Arctic Ocean. The Polar water is in the top layer located from the surface to $150m$ and has its origin in the Arctic Ocean. The temperature of this layer is below $0°C$ near Greenland in both the summer and the winter and is between $2°C$ in the winter and $8°C$ in the summer near Norway. This layer contains a strong halocline. At the surface the salinity is less than 30PSU and at the bottom of the layer the

salinity is 34PSU or more. [35]

Beneath the polar layer is the Atlantic Intermediate Water which originates from the North Atlantic Current. It extends from the bottom of the polar water layer down to about $800m$. The temperature in this layer is above $0°C$ and the maximum temperature is located between 200 to $400m$. The salinity in this layer increases from the polar water values downward until the salinity reaches 34.88 to 35.00PSU at about $400m$. Below that depth the salinity is uniform. [35]

The bottom layer, known as the Deep Water, is $800m$. This water mass is very homogeneous with temperatures below $0°C$ and a salinity between 34.87 and 34.95PSU. It aids in the production of deep water in the Greenland and Norwegian Seas. [35]

The circulation in the Arctic and Sub-Arctic Oceans varies with depth. The discussion of the circulation here is done for each of the layers of the water masses in Arctic Ocean as described above. The circulation of the surface layer is best known. The current's data is mainly derived from sea ice flows and from drift stations [36]. Surface circulation consists of three major paths. The water along the whole Eurasian side of the Arctic Ocean moves towards the pole with a mean speed of 2 to 3 cm/s and then forms part of the East Greenland Current which exits the Arctic Ocean along the Eastern Side of Greenland with an average annual speed of $8cm/s$ [37]. This current is known as the Transpolar Drift. Part of these surface waters travel toward the Beaufort Sea. In the Beaufort Sea they are trapped in a clockwise circulation. This is known as the Beaufort Gyre. The center of the gyre is a $80°N$ and $140°W$ [38].

The circulation of the Atlantic water is driven mainly by baroclinic and bartropic

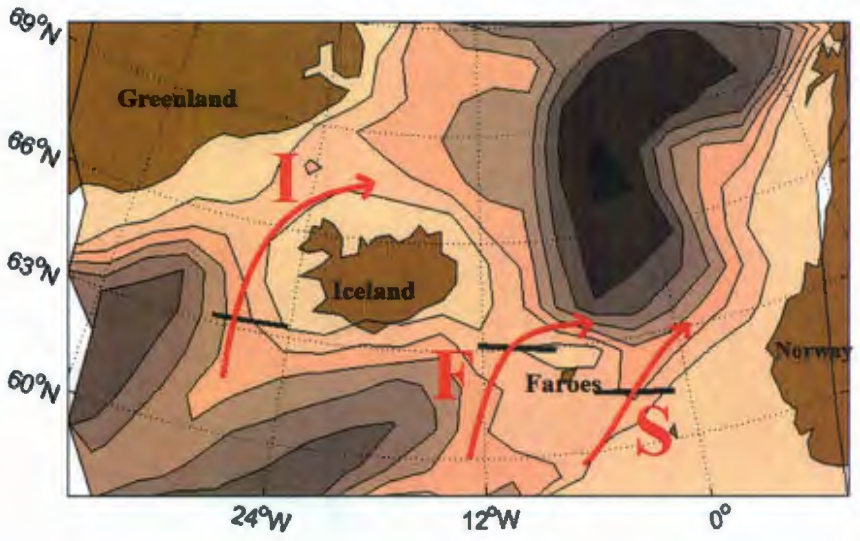

Figure 2.8: The three branches of Atlantic Water that pass over the Greenland-Scotland Ridge. The **I**celand, **F**aroe and **S**hetland Branches

pressure gradients and therefore can be inferred from temperature and salinity [24]. The Atlantic water flows into the Sub-Arctic Ocean by crossing the Greenland-Shetland Ridge. It does so in three branches, named the Iceland, Faroe and Shetland Branches, (see Fig. 2.3). The Iceland Branch travels northward through the eastern most edge of the Denmark Strait, located between Greenland and Iceland. The depth here is about 650m. The southward travelling East Greenland Current passes through the Strait in the western part. The Faroe Branch crosses the ridge between Iceland and Faore Islands. The sill depth here is about 300-480m. The Shetland branch flows along the Scottish coast mainly as a slope current [8]. The sum of these branches forms the total Atlantic inflow in to the Arctic Ocean.

North of the Greenland-Scotland Ridge the main part of the Atlantic water flows along the coast of Norway as a slope current with a speed between 5 and 20cm/s

depending on the season and location [39]. The surface slope current follows the Norwegian coast until approximatly 70^O N where it splits. The smaller part of it turns east and enters the Barents Sea and the rest continues north towards Spitsbergen.

Further north the major portion of the Atlantic water that does not enter the Barents Sea passes through the Fram Strait and the rest recirculates in the Nordic Seas. The Fram Strait is a narrow, deep channel at about 0^OE and 79^ON. It is about 2500m deep and is 400km wide. The deepness of the Fram strait allows the through-flow of the Atlantic Intermediate waters. Only the top 200m of the Atlantic Water can pass though the Barents and Kara Seas where it is exposed to the atmosphere. This is not the case for the Atlantic Water that passes through the Fram Strait and then descends in the Arctic Ocean. The flow through the Fram Strait is northward on the eastern side with a velocity of about $3.0\frac{cm}{s}$ and southward on the western side with a velocity of about $-1.0\frac{cm}{s}$.

The mean net flow through the Fram Strait is 2Sv southward. That is $12Sv$ northward and 14Sv southward [11]. The northward flow of the warm West Spitsbergen Current is in the eastern side of the strait while the cold East Greenland Current is in the western side. In the center there is a westward flow which causes recirculation. The highest velocities are in the upper ($< 1500m$) West Spitsbergen Current with a mean speed above $2.0cm/s$ and maximum speeds of $5.5cm/s$ in the upper $250m$ [11]. The East Greenland Current carries modified Atlantic water southward with a speed of about $1.0cm/s$. Excluding the West Spitsbergen Current the speeds in the Fram Strait are nearly uniform along a vertical section. Warm waters are located in the upper eastern side of the strait while the cold polar waters are located in the upper

western side. At depths greater than $1000m$ the temperature is nearly uniform with a temperature of -0.5 to $1°C$ [11]. The average volume flux of Atlantic water, defined as water above $1°C$, was about 5Sv in the late 1990s and had a maximum of 7Sv in 2005 [11].

The flow of Atlantic Water into the Arctic Ocean is important for several reasons. It transports warm, saline waters which influences the local climate and the thermohaline circulation. The warm water that travels northward keeps the local water warmer and more ice free than it would be otherwise. [40]

The major circulation in this layer in the Arctic Ocean is flow that is parallel to the continental slope and is counter-clockwise. The water in this layer enters the Arctic Ocean west of Spitsbergen and then flows parallel to the continental slope of Eurasia. Some of it heads towards the Lomonosov Ridge and travels in the same direction at the Transpolar drift and the rest of it becomes the outflow along the east of Greenland as an under layer of the East Greenland Current [35] [24]. The speed is about $1 - 5cm/s$ for most of the Beaufort Gyre but are much larger, up to $10cm/s$, immediately north of the Alaska. Mean speed in the Transpolar drift in the central ocean are around $2cm/s$ [24].

Sea ice is formed when the sea water falls below its freezing point. The freezing point of the sea water is determined by its salinity. For example, water with a salinity of 33psu the freezing point is $-1.8°C$. About 14% of the sea ice mass of the Arctic Ocean is exported each year through the Fram Strait [1]. The mean annual area flux of sea ice is $919 \times 10^3 km^2/yr$, which is 10% of the Arctic Ocean area. These fluxes vary interannually with a correspondence to the NAO [41, 42, 43].

In general, there are two different kinds of sea ice, first-year and multi-year ice. First-year ice is in its first winter's growth can have a thickness from very thin (tenths of a meter) to $2.5m$ in the high arctic [2]. The first-year ice that survives the summer's melt become multi-year ice. After each summer that the multi-year survives it becomes harder and fresher. Multi-year ice floes are usually $3m$ thick without ridges [2].

The Arctic sea ice area can be divided into three different regions. They are drifting pack ice, marginal sea ice and land fast ice. The drifting pack ice is mostly perennial and has an area of about 6 million km^2. This pack ice is broken up by leads that vary from 1% in the winter to $10 - 20\%$ in the summer. The average thickness of this perennial pack ice is about $2 - 4m$ but there are pressure ridges which create much greater thicknesses. The marginal sea ice zone is where the pack ice meets the open water. This area shifts with the seasons and is an area of high biological productivity. The last category of sea ice is land fast ice. This ice develops each year along the edges of the continents and islands, mainly the archipelago islands. The edge of this land fast ice can be found at a ocean depth of $22 - 30m$ [19, 2].

The amount of sea ice in the Arctic Ocean changes seasonally. The average maximum sea ice extent is 15 million km^2 in March and the minimum is 7 million km^2 in September [2]. The area of the multi-year ice is about 5 million km^2 and is located mostly over the central ocean, East Siberian Sea and the Canadian polar shelf. The land fast ice is stuck to the shore for about ten months in a year. It is held there by the coast and grounded ice ridges [2]. These grounded ice ridges are a result of pack ice that is repeatedly pushed against the land fast ice and they stabilize the sea ice

for tens of kilometers from the shore. In the CAA this stabilized sea ice can cover an area of 1 million km^2 in late winter and some of it is decades old [2].

Since 2000 there has been an increase in salinity and temperature along all sections. A large variation of temperature and salinity of Atlantic Water also occurred in the 1960s and 70s. The mean volume flux associated with the Atlantic water inflow is 4.3Sv at 62^{O}N at the Norwegian Coast and 1.8Sv for the Barents Sea Opening. There is a linear increase in the volume and heat fluxes through the Barents Sea Opening between 1997 and 2006 by about $0.1\frac{Sv}{year}$; there is no significant trend in the flux in the current at 62^{O}N. [10]

Hansen et al [8] showed that the the Shetland and Faroe branches have higher flows than the Iceland Branch and they reveal a higher temporal variability. The Faroe branch showed a decrease in volume flux between 1950 and 2000 while the Shetland branch showed an increase at the same time which resulted in little to no change in the total Atlantic inflow.

Modeling work done by Karcher et al [12] found that the long term variability of the AW inflow anomalies in to the Northern Seas travel long distances with the circulation. A large volume transport of AW that was anomalously warm into the Nordic Seas over the Greenland-Scotland Ridge in the 1990s lead to record high values of the Fram Strait temperature. Several models agree in the existence of the strong relation of net northward volume flux and NAO during the recent decades [12, 44, 45]. However, Karcher et al found that in the late 1990s the warming was not associated with the strong positive NAO. It was suggested that a study of the heat balances would lead to better understanding of the mechanism for this warming.

Chapter 3

Ocean Model and Experimental Design

The model used in this study is the NEMO-OPA model [20] coupled to the multi-layered ice model NEMO-LIM [46]. Both the ocean model (NEMO-OPA) and sea-ice model (NEMO-LIM) are configured on a global tripolar grid at 2^o horizontal resolution with 31 vertical levels, 20 of which are in the top 500m, (see Fig. 3). This coarse resolution tri-polar grid has two north poles, one over northern Canada and the other over Siberia in order to avoid singularities of the model grid over the ocean (see Fig. 3). The configuration of this grid leads to a horizontal resolution of about 90km within the study region.

Other models are often chosen to be used, such as the NAOSIM hierarchy, which are a group of ocean/sea ice models that are used to study the North Atlantic and Arctic Ocean and the HadCM3 model, which is a coupled ocean and atmosphere model. The NEMO-OPA model is used in this study because it met the requirements

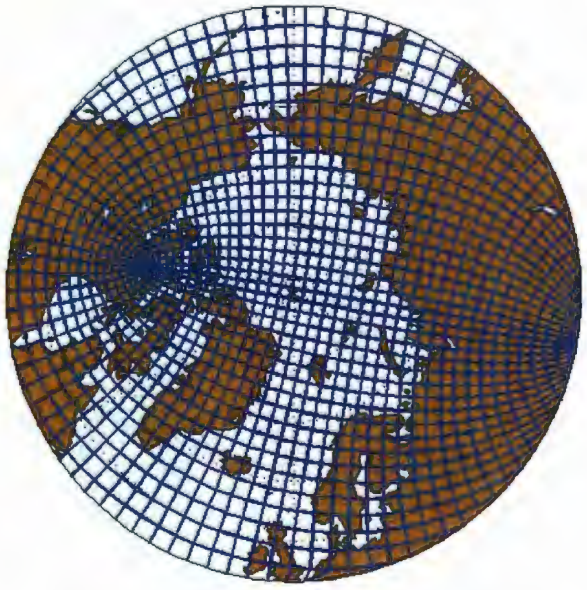

Figure 3.1: The tripolar model grid shown for the study region.

for the needed resolution and speed and its ability to be set up easily on our computing platform.

3.1 The model equations

The governing equations of the model are geophysical fluid dynamics equations on a curvilinear coordinate system. The model assumes the ocean is incompressible, *i.e.*

$$\nabla \cdot \mathbf{U} = 0 \tag{3.1}$$

The Reynold's number is defined as the ratio of advective terms to diffusive terms and simplifies to:

$$Re = \frac{UL}{\nu} \approx \frac{(0.1m/s)(10^5 m)}{10^{-6}m^2/s} = 10^{10} \tag{3.2}$$

The Reynold's number is very large due to the large length scales (L $\sim$ 100km) of the ocean. This means that oceanic flows are always turbulent. Therefore the friction in the model must include turbulent stress and eddies.

The Navier-Stokes equation for an incompressible turbulent fluid in a rotating coordinate system is:

$$\rho \frac{D\mathbf{U}}{Dt} = -\nabla P + \rho \mathbf{g} + \nabla \nu \nabla \mathbf{U} - 2\boldsymbol{\Omega} \times \mathbf{U} \tag{3.3}$$

where $\frac{D}{Dt}$ is the material derivative , ∇ is the gradient, t is the time, z is the vertical coordinate, P the pressure, Ω is the Earth's angular velocity vector, g is the gravitational acceleration, ν is the turbulent viscosity, and ρ is the *in situ* density given by the equation of state

$$\rho = \rho(T, S, P) \tag{3.4}$$

The material derivative in equation 3.3 is defined according to:

$$\frac{D\mathbf{U}}{Dt} = \frac{\partial \mathbf{U}}{\partial t} + \mathbf{U} \cdot \nabla \mathbf{U} \tag{3.5}$$

which after using some vector algebra identities becomes

$$\frac{D\mathbf{U}}{Dt} = \frac{\partial \mathbf{U}}{\partial t} + \frac{\nabla \mathbf{U}^2}{2} + (\nabla \times \mathbf{U}) \times \mathbf{U} \tag{3.6}$$

The small-scale physics for momentum is parametrized by using a turbulent model in the vertical and Laplacian operator in the horizontal. We will use the notation $D_h^u = \nabla \nu \nabla \mathbf{U}$ for the mixing.

The Boussinesq approximation, usually used in ocean models, assumes that the density is equal to the average density,ρ_o, in all equations except the vertical momentum equation, therefore equation 3.3 becomes:

$$\frac{\partial \mathbf{U}_h}{\partial t} + \left[\frac{\nabla \mathbf{U}^2}{2} + (\nabla \times \mathbf{U}) \times \mathbf{U} \right]_h = -\frac{1}{\rho_o} \nabla_h P + \mathbf{D}_h^{\mathbf{U}} - 2\boldsymbol{\Omega} \times \mathbf{U}_h \tag{3.7}$$

where the h subscript denotes that it is the local horizontal vector.

In the vertical we assume that all the terms except the pressure gradient and gravity are negligible. Then we obtain

$$\frac{\partial p}{\partial z} = -\rho g \tag{3.8}$$

which is known as the hydrostatic approximation.

The equations for the conservation of temperature and salinity close the system

$$\frac{\partial T}{\partial t} = -\nabla \cdot (T\mathbf{U}) + D^T \tag{3.9}$$

$$\frac{\partial S}{\partial t} = -\nabla \cdot (S\mathbf{U}) + D^S \tag{3.10}$$

where D^T and D^S are the parametrizations of small-scale physics for temperature and salinity.

The model uses a 2^{nd} order centered advection scheme. In this formulation the value at the velocity points is the mean of the two neighbouring T-point values and is of second order accuracy. The vorticity term in equation 3.7 is calculated using a enstrophy conserving scheme. With this scheme there is a global conservation of enstrophy, $([(\zeta + f)/e_{ef}]^2)$, for a horizontally non-divergent flow [20].

The kinematic boundary conditions are defined at the surface and at solid earth - ocean boundaries. At the bottom mass must be conserved and therefore

$$w = -\mathbf{U}_h \cdot \nabla(H), z = H \tag{3.11}$$

when H is the depth of the ocean at a given location.

At the surface boundary mass conservation gives

$$w = \frac{\partial \eta}{\partial t} + \mathbf{U}_h|_{z=\eta} \cdot \nabla_h(\eta) + P - E, z = 0 \tag{3.12}$$

where $P - E$ is the mass flux of freshwater into the surface. Using equation 3.11, 3.12 and the continuity equations we find the free surface equation

$$\frac{\partial \eta}{\partial t} = \nabla \cdot \left[(H + \eta)\bar{\mathbf{U}} + P - E\right] \tag{3.13}$$

which is used to calculate the height of the ocean free surface.

The wind stress is calculated from the bulk formulas

$$\tau = \rho C_D U_{10}^2 \tag{3.14}$$

where τ is the wind stress, ρ is the density of the air, C_D is the drag coefficient of the surface and U_{10} is the wind speed at $10m$ above the surface. Over the ocean there is a

lower coefficient of friction than over regions with highly ridged sea ice. The dynamic boundary condition at the surface is [20]:

$$\tau_x = \nu \frac{\partial u}{\partial z}, z = 0 \tag{3.15}$$
$$\tau_y = \nu \frac{\partial v}{\partial z}, z = 0$$

No slip boundary condition is defined at the bottom boundary is defined:

$$u = v = 0 \tag{3.16}$$

The temperature and salinity surface flux boundary conditions are given by

$$\begin{aligned} \frac{\partial T}{\partial t}|_{z=0} &= \frac{Q_{ns}}{\rho_o C_p e3t} \\ \frac{\partial S}{\partial t}|_{z=0} &= \frac{EMP\ S|_{z=0}}{e3t} \end{aligned} \tag{3.17}$$

respectively [20]. Where Q_{ns} is the heat flux absorbed at the surface and includes the sensible, latent and long wave radiatvie fluxes. EMP is the total surface fresh-water budget, evaporation - precipitation - river runoff + change is sea ice thickness. The heat capacity is C_p and $e3t$ is the depth of the first model layer. The short wave radiative flux penetrates below the surface and is absorbed in the water column.

3.2 Model Grid

The model is configured on a standard staggered Arakawa C grid. The scalar grid points are denoted by t, vector grid points are denoted by u and v and the vorticity grid points are denoted by f. The different grid point are shifted by a half step as shown in Fig. 3.2.

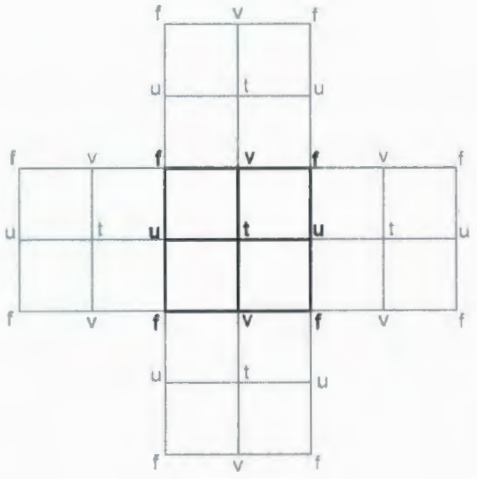

Figure 3.2: Arakawa C-grid.

The scale factors define the local metrics of the curvilinear tri-polar grid. They are defined as the distance between the grid points. In the both the north-south direction and the east-west directions they are given by:

$$\begin{aligned} e_1 &= (a+z)\left[\left(\frac{\partial\lambda}{\partial i}\cos\phi\right)^2+\left(\frac{\partial\phi}{\partial i}\right)^2\right]^{1/2} \\ e_2 &= (a+z)\left[\left(\frac{\partial\lambda}{\partial j}\cos\phi\right)^2+\left(\frac{\partial\phi}{\partial j}\right)^2\right]^{1/2} \\ e_3 &= \left(\frac{\partial z}{\partial k}\right) \end{aligned} \tag{3.18}$$

where a is the radius of the earth, z is a altitude above a reference sea level, λ is the longitude and ϕ is the latitude. Within the thin-shell approximation $(a+z)$ can be replaced by a. [20]

Partial steps are used along the bottom topography. Without using the partial steps the bottom topography is divided up into discrete steps that have the size of the

model vertical levels. These larger steps can misrepresent a shallow sloped bottom or large localized depth gradients and this can lead to large localized vertical velocities which leads to numerical dispersion effects. Therefore, partial steps are used to better represent the topography [20, 47].

The model's salinity and temperature profiles were initialized using monthly averaged Levitus salinity and temperature [48]. In order to reduce model drift and bias on the climatological time scale a spectral nudging scheme is applied [49]. The nudging is applied to the surface layers above 45°N for salinity only so as to not affect the interannual variability in the intermediate waters in which we are concerned.

3.3 Forcing and Ensemble model runs

The model forcing is computed from bulk parametrization of the surface turbulent heat, momentum and water fluxes. These turbulent fluxes are computed with model SST, near surface atmospheric temperature, wind speed, humidity and precipitation using the bulk formulae. They relate the wind stress(τ), sensible heat(SH) and latent heat(LH) to the measured quantities of the atmosphere.

$$\begin{aligned} \tau &= \rho_{atm} C_d (u_{atm} - u_s) \\ SH &= \rho_{atm} C_h (T_{atm} - T_s) \\ LH &= \rho_{atm} C_e u (q_{atm} - q_s) \end{aligned} \tag{3.19}$$

Where ρ_{atm} is the surface air density, $u_{atm}, T_{atm}, q_{atm}$ are the wind speed, temperature and specific humidity respectively at $10m$. $u_{atm}, T_{atm}, q_{atm}$ at $10m$ can be calculated

from wind, temperature and humidity at any height and stratification using profile relationships. The 's' subscript means the value at the surface. In these formulas u_s is assumed to be zero and q_s is the saturation humidity at T_s multiplied by 0.98 because of the reduced saturation of the specific humidity due to being over salt water. The coefficients C_d, C_h, C_e are determined empirically. The total cloud cover is used to calculate the surface radiative balance.

Ocean models are not a perfect representation of the actual physics that occurs in the ocean. They are many parametrizations in the models and therefore there is error associated with the model itself. The coarseness of this model allows for an ensemble of runs to be possible. Using different initial conditions for each ensemble member the model's error in the results can be studied. In this thesis all results presented are the raw mean of the ensemble members and the error bars given are the 95% confidence level in the ensemble unless otherwise stated.

The atmospheric parameters used in this study are from NCEP/NCAR reanalysis. Two data sets of these parameters are used in this study: they are monthly mean data and 6-hourly NCEP/NCAR data for the period 1948-2005. The model is first spun-up for 30years using climatological atmospheric conditions as the forcing. The model is then run for 50 years, from 1948-2005, using the 6 hourly NCEP/NCAR forcing. A 'snap-shot' is saved every year during this run. Six of these 'snap-shots' were then chosen to be the initial conditions for each of the ensemble members, the first one after another 37 years of spin-up. The initial conditions are chosen so as to have a spread of intensities and sign of the North Atlantic Oscillation (NAO) index. The chosen years were 1985, 1989, 1992, 1994,1996,and 1997. Each of these 6 initial

conditions were used to the ensemble from 1948-2005 saving the output monthly for analysis. The output from 1965-2005 is used for analysis in this study.

Chapter 4

Simulation of the Arctic and Sub-Arctic Ocean Climate

This chapter presents results from simulations of climate characteristics of the Arctic and Sub-Arctic Oceans. The simulated water mass properties and circulation are discussed and the skills of the model to represent the climate of these regions are assessed. The results from the model simulations are present for the Sub-Arctic Ocean (section 4.1) , the Arctic Ocean (section 4.2) and the main straits (section 4.3). These regions are shown in Fig. 4.1.

4.1 Climate of the Sub-Arctic

The Polar water in the Greenland-Norwegian Seas has a temperature that is below 0°C near Greenland in the summer and the winter and is between 4°C and 6°C in the winter and 14°C in the summer near Norway (see Fig. 4.2a and 4.2b). These tem-

Figure 4.1: Sections used to study climatic characteristics and variability of fluxes in and out of the Nordic and Sub-polar seas. F- Fram Strait, BSO- Barents Sea Opening, GS- Greenland Scotland Ridge.

peratures near Norway are warmer than expected from observations. At the surface the salinity is between 32PSU and 35PSU or more in both the winter and summer (Fig. 4.3a and 4.3b) . The salinity here is expected to be lower, less than 34PSU from observations. The coarse resolution of the model was not able to completely capture the narrow East Greenland Current and therefore did not simulate the lower temperature and salinity perfectly.

Beneath the Polar Water layer is the Atlantic Intermediate Water. It extends from the bottom of the polar water layer down to about $800m$. The temperature in this layer is above 0^oC always, as expected from observations, and the maximum temperature is 8^oC in the winter and 14^oC in the summer (see Fig. 4.2c and 4.2d). The salinity in this layer is between 34.4 and 35.3PSU in both the summer and winter, while the observed range of 34 to 35.00PSU is slightly fresher.

The bottom layer, known as the Deep Water, below $800m$ is observed to be below 0^oC and the salinity between 34.87 and 34.95PSU in the Nordic Seas. Our simulated Nordic Seas temperature is between 0^oC and 2^oC in both winter and summer(Fig. 4.2e and 4.2f) while the simulated salinity is as in observations (Figs. 4.3e and 4.3f). In Fig. 4.2e and 4.2f the separation of the water masses by the Greenland- Scotland Ridge is seen. The temperature of the Deep Water in the sub-polar sea is warmer, $3^o < T < 6^oC$, than in the Nordic Seas.

There is a large gradient in the temperature and salinity between the relatively short distance between the Greenland and Norwegian coasts and therefore there is a large gradient in the density. This has an impact on the major currents of the Nordic Seas. There is counter-clockwise flow in the middle of the Nordic Seas at both the

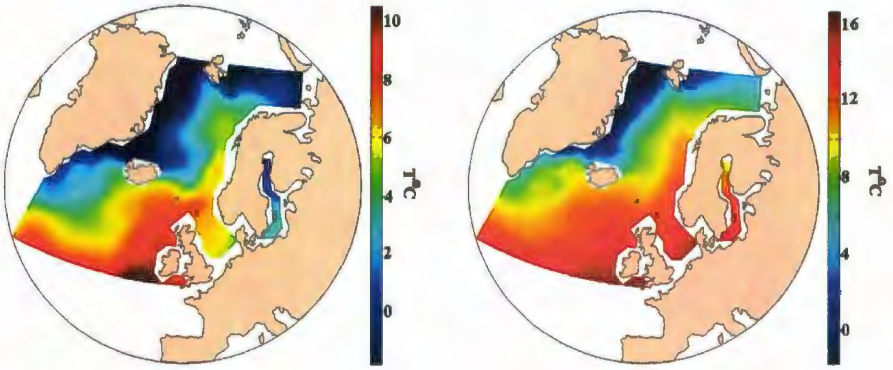

a Temp. of surface in winter

b Temp. of surface in summer

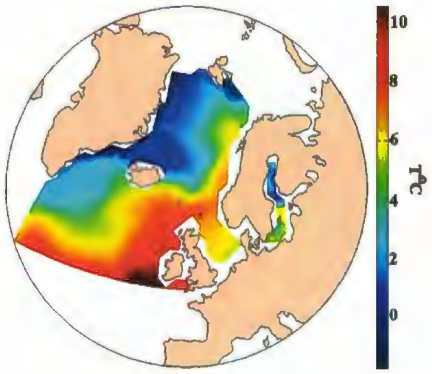

c Temp. of AW layer in winter

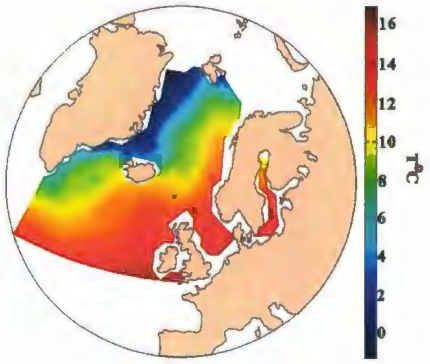

d Temp. of AW layer in summer

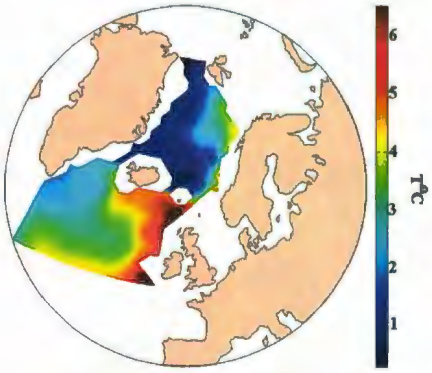

e Temp. of bottom layer in winter

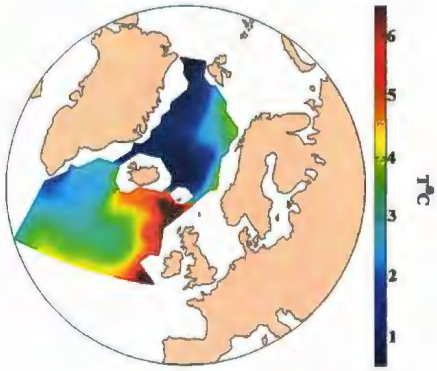

f Temp. of bottom layer in summer

Figure 4.2: Temperature of the Surface Water in the winter (a) and summer(b), the Atlantic Intermediate Water Layer in the winter (c) and summer(d) and at $1830m$ in the summer (e) and winter (f) of the Sub-Arctic.

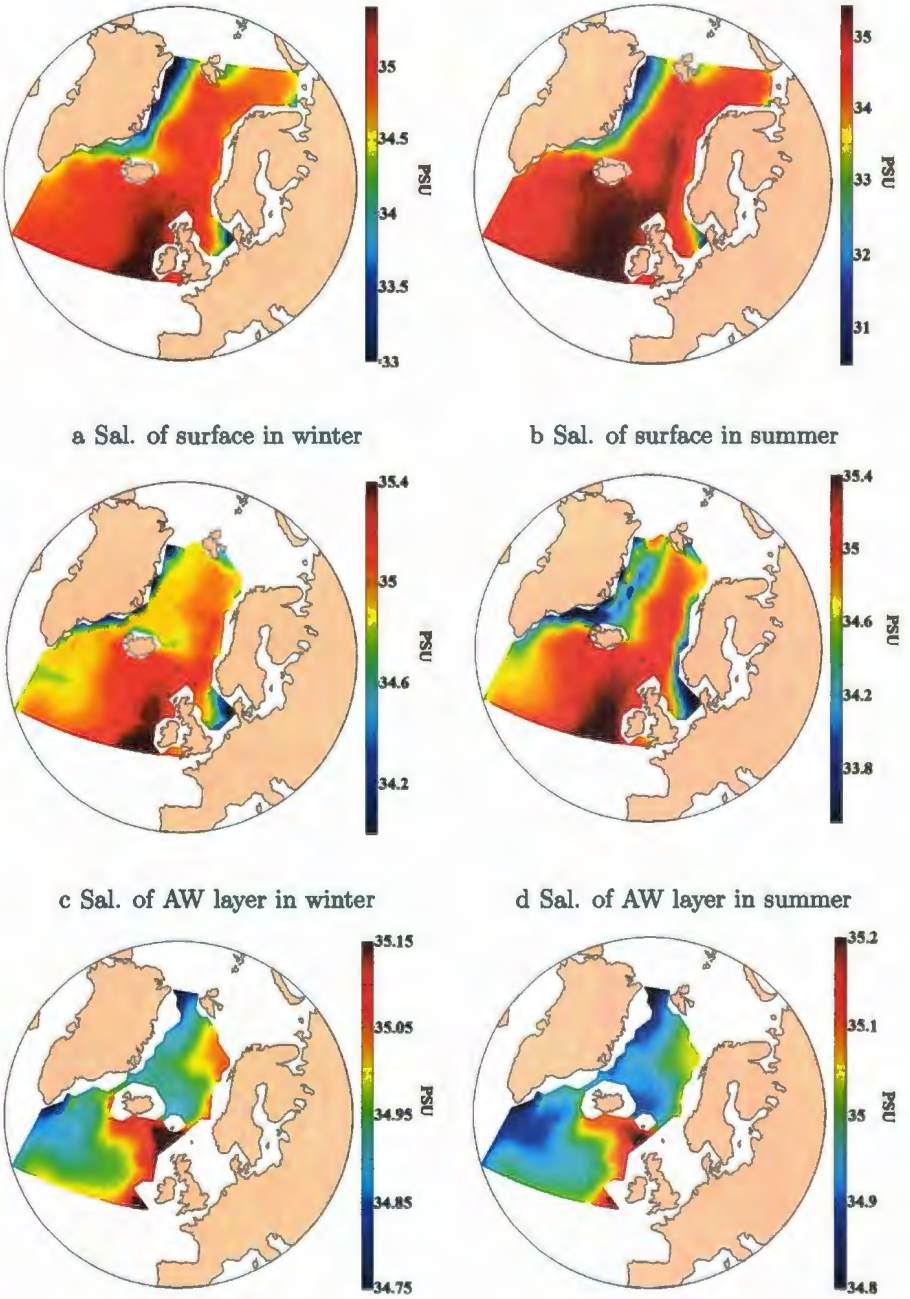

a Sal. of surface in winter

b Sal. of surface in summer

c Sal. of AW layer in winter

d Sal. of AW layer in summer

e Sal. of bottom layer in winter

f Sal. of bottom layer in summer

Figure 4.3: Salinity of the Surface Water in the winter (a) and summer(b), the Atlantic Intermediate Water Layer in the winter (c) and summer(d) and at $1830m$ in the summer (e) and winter (f) of the Sub-Arctic.

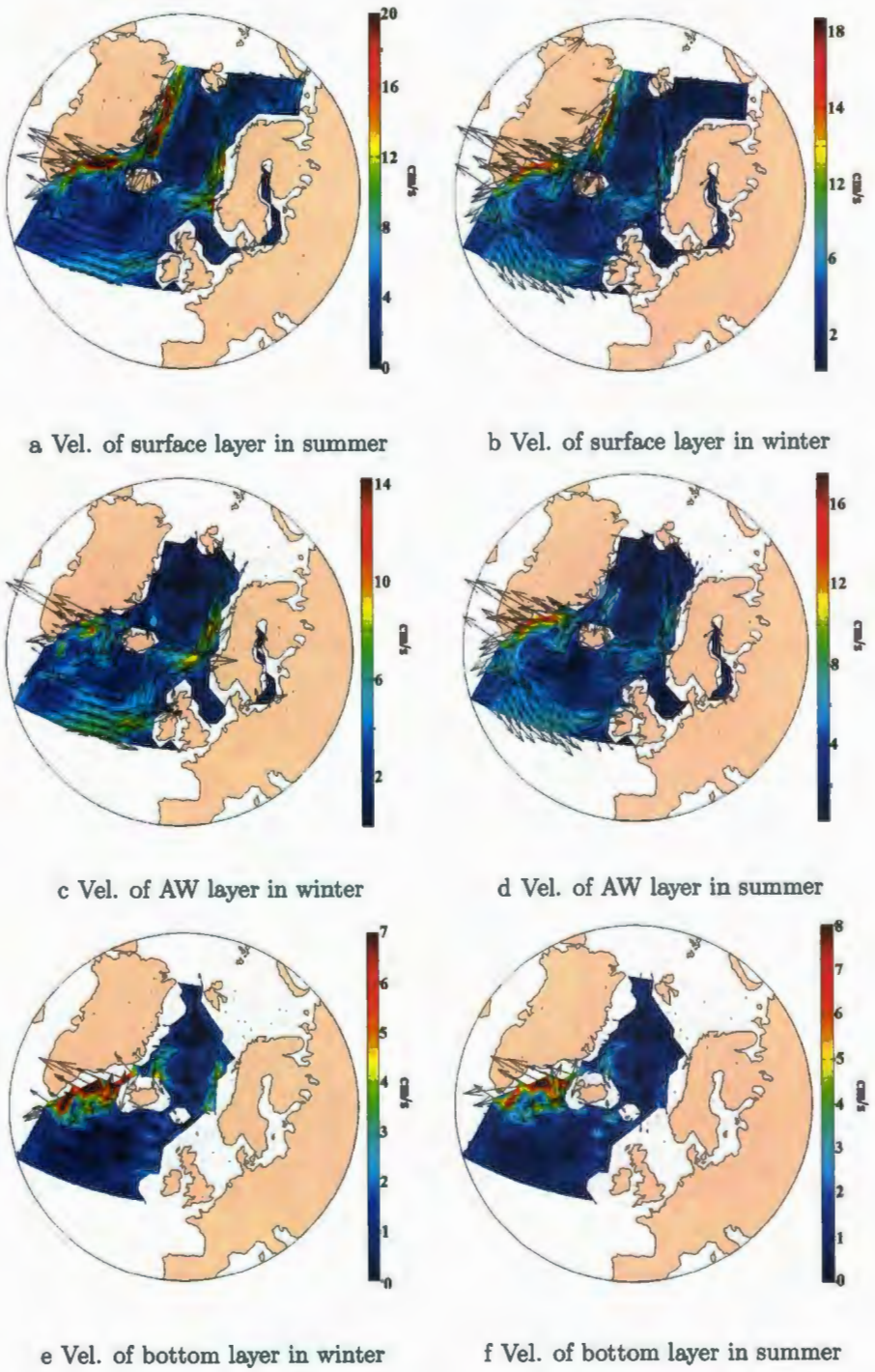

a Vel. of surface layer in summer

b Vel. of surface layer in winter

c Vel. of AW layer in winter

d Vel. of AW layer in summer

e Vel. of bottom layer in winter

f Vel. of bottom layer in summer

Figure 4.4: Current Velocity in the Surface Water in the winter (a) and summer(b), the Atlantic Intermediate Water Layer in the winter (c) and summer(d) and at $1830m$ in the summer (e) and winter (f) of the Sub-Arctic.

surface and the Atlantic water layer as expected from observations (see Fig. 4.4a, 4.4b,4.4c,4.4d). The centre of this rotating flow is further west at the Atlantic water layer than at the surface. From figurs 4.4c and 4.4d the three branches of flow over the Greenland-Scotland can be seen, along the west coast of Iceland, around Faroes and along the Scottish shelf edge at the Atlantic water layer. The fastest currents in the surface layer are located along the Scottish shelf, $+8cm/s$, and along the coast of Greenland, $-8cm/s$ as expected from observations. The flow along the Scottish shelf is expected from observations to be between 5 and $20cm/s$. At the Atlantic water layer the fastest currents are again located along the Scottish shelf, $+8cm/s$, and along the Southeastern coast of Greenland, $-7cm/s$

As expected the model results show the Atlantic water current north of the Greenland-Scotland Ridge flows along the coast of Norway as a slope current. The surface slope current follows the Norwegian coast until approximately 70^O N where it splits. Part of it turns east and enters the Barents Sea and the rest continues north towards Spitsbergen. The bottom layer is modeled to be slightly, $\approx 1cm/s$, slower than expected from observations.

The velocities of the surface currents are slower in the summer (figure 4.4b) than in the winter (figure 4.4a) along the coasts of Greenland and Norway and faster in the summer at the Atlantic Water Layer (see Fig. 4.4d and 4.4c). There is negligible change in the Deep water velocities between seasons (see Fig. 4.4f and 4.4e).

4.2 Climate of the Arctic

The temperature of the surface water ranges from -1.82 to -1.66^{o}C in the winter. The temperature is at the freezing point everywhere in the winter and it is clear that freezing point of the water corresponds to the salinity at that location (see Fig. 4.5a and 4.6a). In the summer, when there is less ice, the water warms to -1.7 to -0.9^{o}C (see Fig. 4.5b) which is slightly cooler than the expected temperature from observations of up to 0^{o}C. The Atlantic Water is beneath the Surface water and is located between 200 and $900m$. The temperature at this layer ranges between -0.25 to 0.5^{o}C in the winter (see Fig. 4.5c) and to 0.85^{o}C in the summer (see Fig. 4.5d). The observed range is from -1 to 0.5^{o}C. Below the Atlantic Water is the Bottom Water. Its temperature everywhere is below 0^{o}C, as expected from observations, and has minimum temperatures ranging from -0.4 to 0^{o}C with the cooler temperature in the Eurasian Basin as expected from observations (see Fig. 4.5e and 4.5f).

The Surface Arctic Water salinity varies between 30.5 and 31.5 PSU (see Fig. 4.6a and 4.6b) near areas of freshwater influx such as a large river or the Bering Strait. These waters are about 2PSU saltier than expected from observations. The salinity is between 32 and 34 PSU (see Fig. 4.6a and 4.6b) in regions where the water is influenced by advection Atlantic water. The salinity of the Atlantic Water layer is $34.4-34.8$ PSU in the summer (see Fig. 4.6d) and $34.6-34.85$ PSU in the winter(see Fig. 4.6c). These simulated values are fresher than the observed range of 34.9to35 PSU in the Arctic Ocean. The observed salinity of the bottom layer is between 34.92 and 34.99PSU. The model simulated salinity is fresher, ranging from 34.6 to 34.9PSU (see Fig. 4.6e and 4.6f).

Surface circulation consists of three major paths. The water along the whole Eurasian side of the Arctic Ocean moves towards the pole with a mean speed of 2 to 5 cm/s and then forms part of the East Greenland Current which exits the Arctic Ocean along the Eastern Side of Greenland with an average speed of $8cm/s$ in the summer (see Fig. 4.7b) and $11cm/s$ in the winter(see Fig. 4.7a).

The highest velocity in the Atlantic Water Layer is located along the Russian shelf edge as part of what was the West Spitsbergen Current, as expected from observations. It has a mean speed of $2-3cm/s$ in both the winter and summer as in observations (see Fig. 4.7c and 4.7d).

In the Atlantic Layer and at $1830m$ the Beaufort gyre is no longer distinguishable and the greatest currents are the water circulation of the Eurasian basin. In the bottom layer the currents are very slow ($\approx 0.5cm/s$) when compared with the surface waters (see Fig. 4.7e and 4.7f). This leads to a long residency of the bottom waters.

As we know the sea of the Arctic is important. One important measure of sea ice is the sea ice extent, shown in figure 4.8 where the modelled and observed are compared. Due to differences between the resolution and area covered in observations and in model datasets the magnitude of the sea ice extent differs between the two. Therefore, the normalized anomaly of the sea ice extent for the two are shown. Excluding the two large deviations in 1980 and 1990 the linear trend of the modelled and observed is similar. The difference between the slope of the modelled and observed sea ice extent is statistically insignificant ($p>0.1$).

The sea ice extent also varies seasonally. The average seasonal cycle of sea ice extent is shown in Fig. 4.9. The maximum sea ice extent is in March of the year and

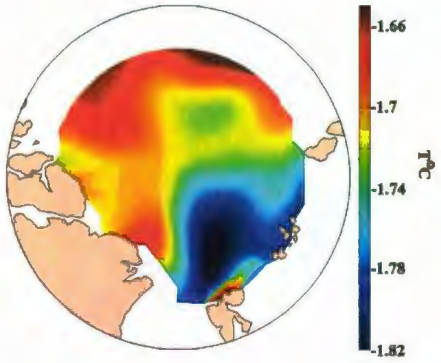

a Temp. of surface layer in winter

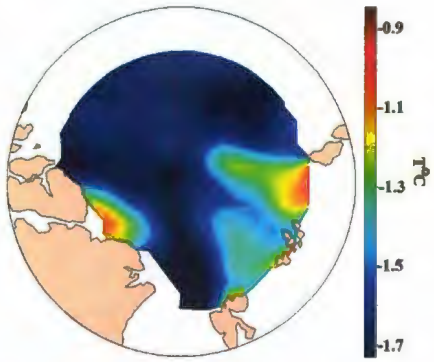

b Temp. of surface layer in summer

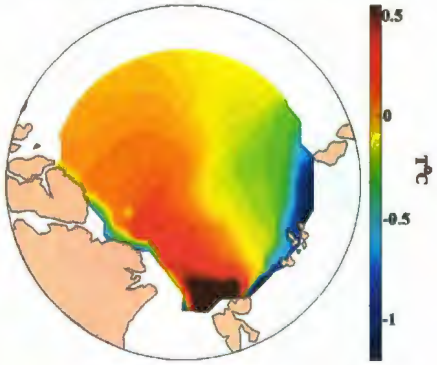

c Temp. of AW layer in winter

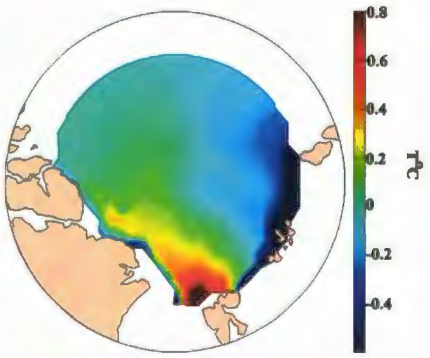

d Temp. of AW layer in summer

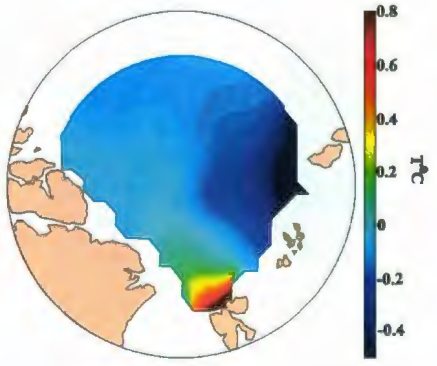

e Temp. of bottom layer in winter

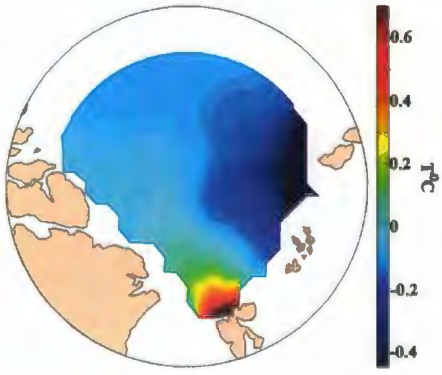

f Temp. of bottom layer in summer

Figure 4.5: Temperature of the Surface Water in the winter (a) and summer(b), the Atlantic Water Layer in the winter (c) and summer(d) and at $1830m$ in the summer (e) and winter (f) of the Arctic.

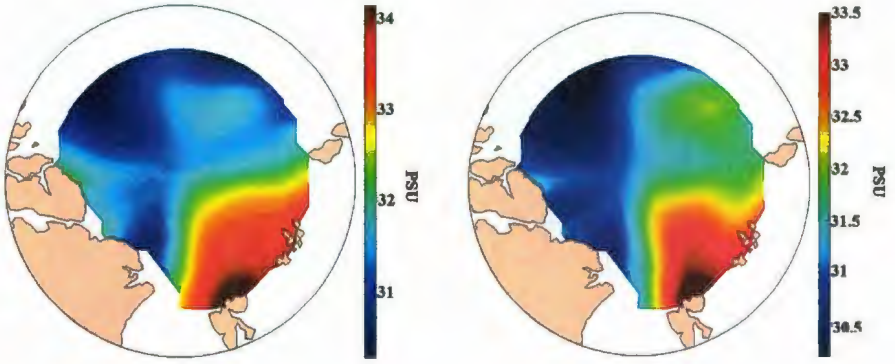

a Sal. of surface layer in winter

b Sal. of surface layer in summer

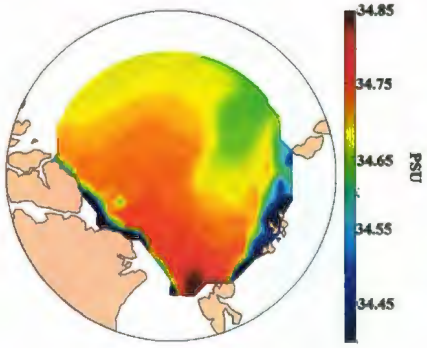

c Sal. of AW layer in winter

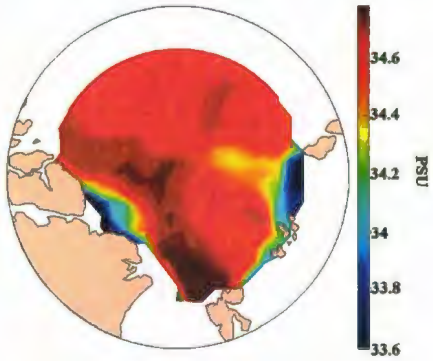

d Sal. of AW layer in summer

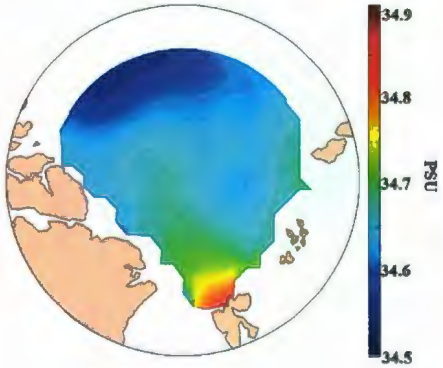

e Sal. of bottom layer in winter

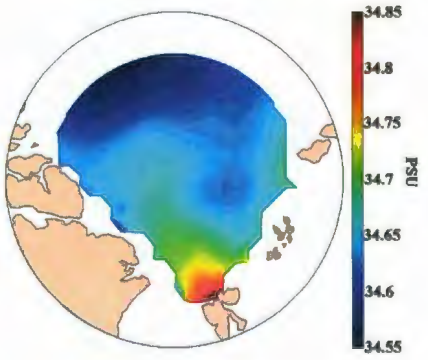

f Sal. of bottom layer in summer

Figure 4.6: Salinity of the Surface Water in the winter (a) and summer(b), the Atlantic Water Layer in the winter (c) and summer(d) and at $1830m$ in the summer (e) and winter (f) of the Arctic.

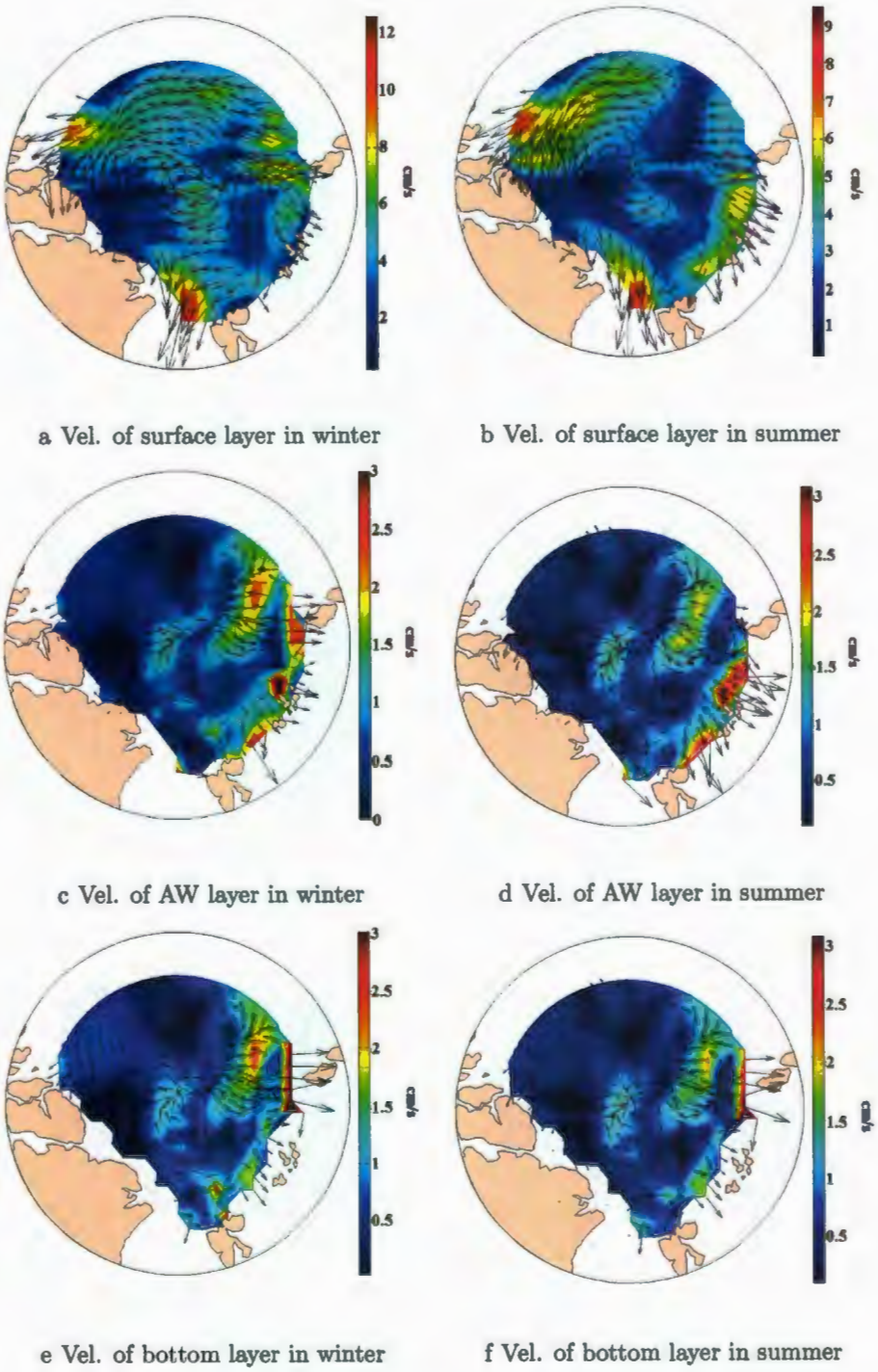

a Vel. of surface layer in winter

b Vel. of surface layer in summer

c Vel. of AW layer in winter

d Vel. of AW layer in summer

e Vel. of bottom layer in winter

f Vel. of bottom layer in summer

Figure 4.7: Current Velocity in the Surface Water in the winter (a) and summer(b), the Atlantic Water Layer in the winter (c) and summer(d) and at $1830m$ in the summer (e) and winter (f) of the Arctic.

minimum extent is in late summer. The minimum extent occurs one month earlier for the model than the observations. The model also underestimates the extent in the summer (May-Aug) and overestimates in the fall (Sept-Dec). However, the model and observation are close with a correlation of 0.8675 ($p<0.01$) and when shifted by one month the correlation is 0.9206 ($p<0.01$).

4.3 Climate of the Straits

The Atlantic water flows into the Arctic Ocean by crossing the Greenland-Shetland Ridge from the Sub-polar section. It does so in three branches, the Iceland, Faroe and Shetland Branches, which can be seen in Fig. 2.3. Figures 4.10a and 4.12a show the warm and salty Atlantic Water which travels northward in the branch locations.

The water is warmest and saltiest on the eastern side of the Greenland-Scotland Ridge. The coldest and freshest water is on the western-most edge of the strait which is the East Greenland Current. The over-flow water mass is also visible in Fig. 4.10a as expected from observations. The cool over-flow water flows from the Nordic Seas to the sub-polar ocean. This over-flow water is an important contributor to deep convection that occurs in the sub-polar seas. The temperature through the Fram Strait, Fig.4.10b clearly shows two water masses. The higher temperature, salty AW with $T> 1°C$ on the eastern side and the cold, fresh Polar water with $T< 0°C$ on the western side.

Observations show that the temperature of the water through the Fram Strait is warmest in the later part of the each year and cooler in the beginning [11]. The model

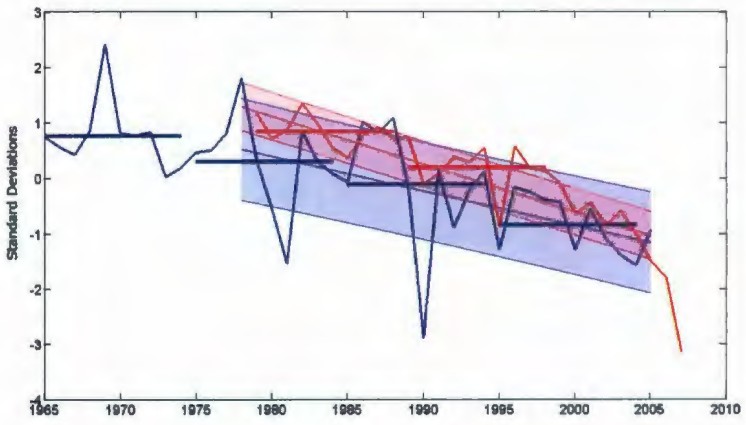

Figure 4.8: Variability of Arctic sea ice extent. The modelled normalized anomaly of the sea ice extent is blue and the observations [50] are red.

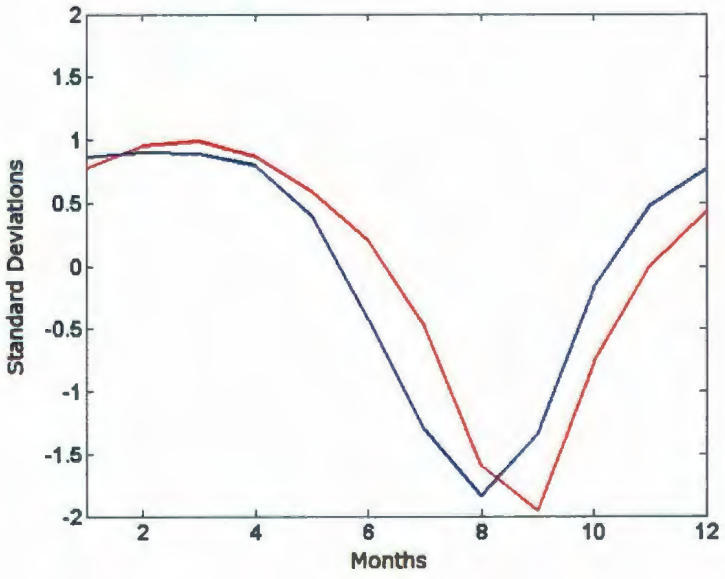

Figure 4.9: Average Seasonal cycle of the Arctic sea ice extent. The modelled normalized anomaly of the sea ice extent is blue and the observations [50] are red.

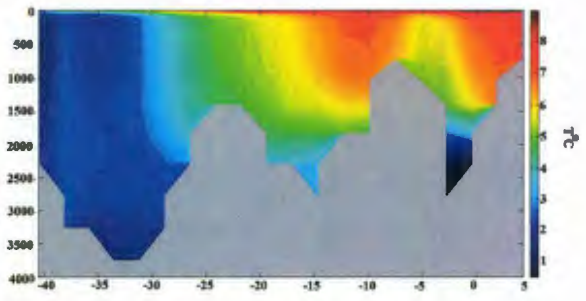

a Greenland-Scotland Ridge Temp.

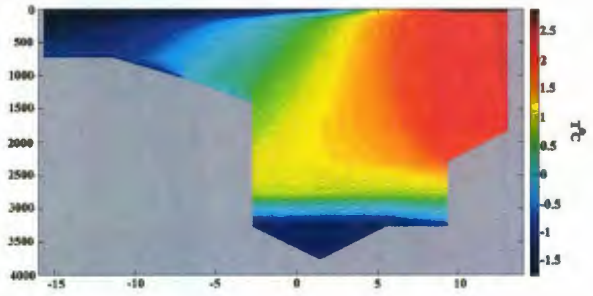

b Fram Strait Temp.

Figure 4.10: Temperature cross sections along the (a) Greenland-Scotland Ridge and (b) Fram Strait. Please note the different scales.

was able to reproduce this seasonality in the average temperature and the magnitude of the interannual variability.

The observed northward volume flux through the Fram Strait is 12 ± 1Sv [11]. It is lower, 7.5 ± 0.7 Sv in the model results. Similarly, the southward volume flux from observations is 14 ± 1Sv and is 10.7 ± 0.6 Sv from model results. The total volume flux through the Fram Strait calculated from model results is 3.1 ± 1Sv and the from observations is 2 ± 2Sv [11].

The Fram Strait is a narrow passageway and our model has a coarse resolution. In

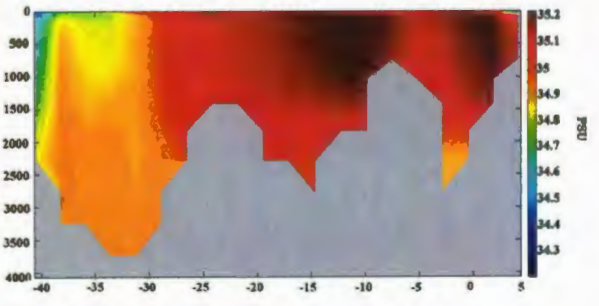

a Greenland-Scotland Ridge Sal.

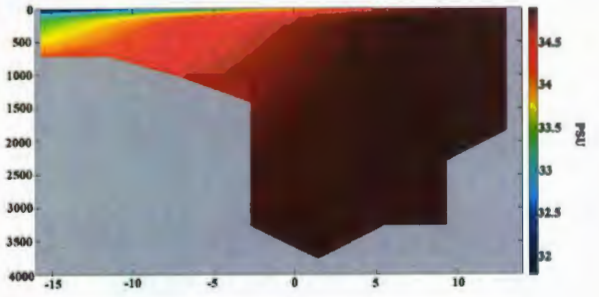

b Fram Strait Sal.

Figure 4.11: Salinity cross sections along of the Greenland-Scotland Ridge.

order to allow for proper flow through the Fram strait it is artificially deepened, this is a common practice for coarse resolution models. This deepening is the most likely the cause for the difference in the magnitudes of the Northward and Southward flows between observations and model while the total flow from the model and observations are within error of each other.

The flow through the Fram Strait is northward on the eastern side with an observed velocity of about $3\frac{cm}{s}$ and southward on the western side with an observed velocity of about $-1\frac{cm}{s}$. The velocities from the model are higher,$-5\frac{cm}{s}$ to $4\frac{cm}{s}$, as seen in Fig. 4.12b. The northward flow is warm and salty (about 5^{O}C and 35 PSU) and

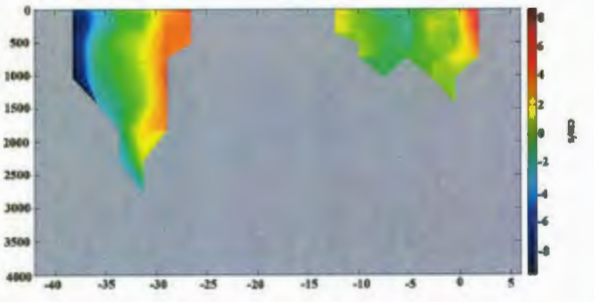

a Greenland-Scotland Ridge Vel.

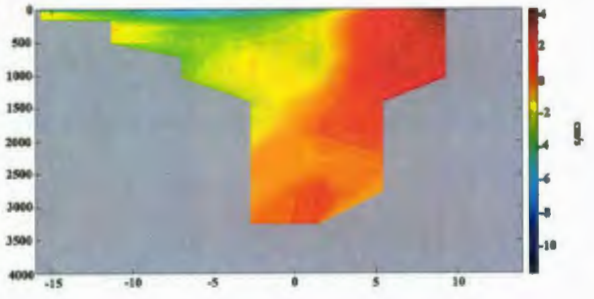

b Fram Strait Vel.

Figure 4.12: Velocity cross sections along the (a) Greenland-Scotland Ridge and (b) Fram Strait.

the southward flow is colder and fresher (about -2^{O}C and 34 PSU) especially in the top $500m$ as seen in Fig. 4.10b and 4.11b. Below this depth the water is much more uniform with a temperature between 0 and -1^{o}C and a salinity of 34.9 PSU.

The volume flux of just the Atlantic Water (AW) is calculated using

$$V_A(t) = \sum_k \sum_j A_{k,j} u_{k,j}(t) \beta_{k,j}(t) \tag{4.1}$$

where the sum is over all the grid-points within the section. $\beta_{k,j}(t)$ is the fraction of the Atlantic water in that box and $u_{k,j}(t)$ is the velocity. The velocity is provided

by the model, therefore only $\beta_{k,j}(t)$ needs to be calculated. The Greenland-Scotland Ridge is divided up into three sections and the fraction, β, is calculated differently for each one because the properties of the AW varies along the length of the ridge. The flux of the AW across the entire ridge is estimated in three parts. First, by calculating the flux for the Iceland Branch across the 64°N parallel between Iceland and Greenland, 28°W to 23°W. The second part, the Faroe Branch, is between Iceland and the Faroe Islands, at 62°N 12.5°W to 7^oW. The third part, the Shetland Branch, is from the Faroe Islands to Shetland, at 61.5°N 7.5°W to 0^oW.

Following the work of Hansen et.al [51] the Faroe and Shetland branches fraction, $\beta_{k,j}(t)$, is calculated using a 3 point mixing model. We assume that the AW mixes with Modified Icelandic Water (MIW) and Nordic Sea water (NSW) in the Shetland and Faroes Sections and so the 3 mixing equations are

$$\begin{aligned} m_{AW}T_{AW} + m_{MIW}T_{MIW} + m_{NSW}T_{NSW} &= T \\ m_{AW}S_{AW} + m_{MIW}S_{MIW} + m_{NSW}S_{NSW} &= S \\ m_{AW} + m_{MIW} + m_{NSW} &= 1 \end{aligned} \tag{4.2}$$

The fraction of AW is calculated by solving the above system of equations for m_{AW}, where T and S are the temperature and salinity of the strait. Similarly, in the Iceland Branch we assume the AW mixes only with the Polar Water (PW) and so the fraction of Atlantic Water is calculated using a simple mixing model, *i.e.* by solving the systems of equations below. Table 4.1 shows how the water masses were defined in the various sections.

Branch	Temperature (^{o}C)	Salinity (PSU)
Iceland	$T_{AW} = 7.5 + (0.9\cos(\frac{2\pi}{12}(mth - 9))$ $T_{PW} = 0.7 + (1.25\cos(\frac{2\pi}{12}(mth - 9))$	Not needed for 2-point mixing model
Faroe	$T_{AW} = 9 + (0.58\cos(\frac{2\pi}{12}(mth - 9))$ $T_{NSW} = 0.5$ $T_{MIW} = 3$	$S_{AW} = 35.23 + (0.02\cos(\frac{2\pi}{12}(mth - 8))$ $S_{NSW} = 34.9$ $S_{MIW} = 34.8$
Shetland	$T_{AW} = 9.89 + (0.53\cos(\frac{2\pi}{12}(mth - 9))$ $T_{NSW} = 0.5$ $T_{MIW} = 1.5$	$S_{AW} = 35.40 + (0.018\cos(\frac{2\pi}{12}(mth - 8))$ $S_{NSW} = 34.9$ $S_{MIW} = 34.8$

Table 4.1: Table of water mass temperature and salinity used to calculate the fraction of Atlantic Water through the various sections of the Greenland-Scotland Ridge. Values are from Hansen [51]

$$\begin{aligned} m_{AW}T_{AW} + m_{PW}T_{PW} &= T \\ m_{AW}S_{AW} + m_{PW}S_{PW} &= S \\ m_{AW} + m_{PW} &= 1 \end{aligned} \tag{4.3}$$

The volume flux of the AW calculated for each branch from the model results are with in error of observations [8] as show in table 4.2. The temperature of the AW in all of the branches over the Greenland-Scotland Ridge is about 0.5 to 1.5^{o}C, cooler for the model results than for the observations. The modelled salinity in each branch

	Modeled			Observations		
Branch	**Vol. (Sv)**	**T°C**	**Salinity**	**Vol.(Sv)**	**T°C**	**Salinity**
Iceland	1.3 ± 0.3	5.5 ± 0.8	35.10 ± 0.03	0.8 ± 1	6	< 35
Faroe	6 ± 3	6.8 ± 0.5	35.21 ± 0.04	3.8 ± 1	8.2	35.23
Shetland	5.9 ± 3	8.6 ± 0.6	35.28 ± 0.02	3.8 ± 1	9.5	35.32
Total Atl.	13 ± 6	6.7 ± 0.6	35.19 ± 0.03	8.5	8.5 ± 3	35.25

Table 4.2: Table of model and observed [8] Greenland-Scotland Ridge Atlantic Water characteristics

is close to that of the observations.

The majority of the AW passes through the Faroe and Shetland Branches. The flow through the I Branch is cooler and fresher than the other two due to the close proximity of the cold, fresh East Greenland Current.

Chapter 5

Simulation of Interannual and Decadal Variability of Arctic and Sub-Arctic Ocean

5.1 Variability of the Sub-polar Region

The Sub-Polar Region is an important contributor to the global ocean water and heat transport. The deep convection in the Labrador Sea forms the Labrador Sea Water. This water mass together with the modified Denmark Strait and Iceland-Scotland overflows contribute to the North West Atlantic Deep Water which feeds the deep components of the meridional over turning circulation. Recent studies [52, 53] demonstrated that the processes of deep water formation and circulation in the sub-polar gyre have shown a strong interannual variability in the last 40 years. Here we discuss this variability and its impact on the rest of the sub-Arctic and Arctic Oceans.

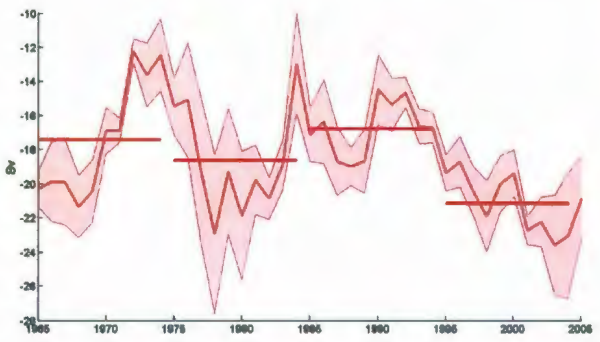

a Volume Flux

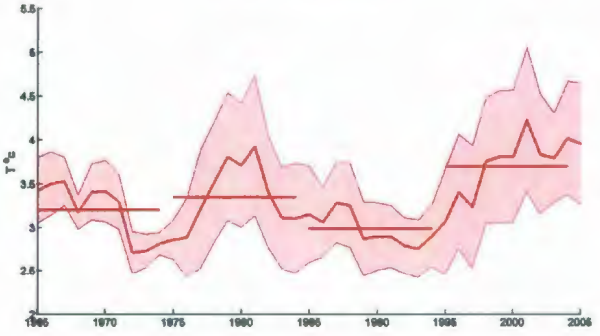

b Temperature

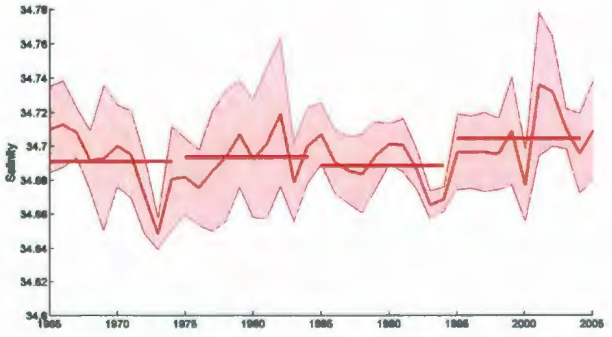

c Salinity

Figure 5.1: Varability of (a) total volume flux , (b) temperature and (c) salinity in the South Greenland section.

The two sections discussed here are the South Greeland section and the South Sub-Polar Section, shown in Fig.4.1. Previous studies showed that the transport in the sub-polar gyre (SPG) decayed in the late 1990s [54]. The South Greenland section transects the SPG and therefore the flow through this section gives a measure of the state of the SPG. My model results reproduce this weakening (Figs. 5.1a,5.1b,5.1c) and its impact on the observed increase in temperature (Fig. 5.1b) and in salinity (Fig. 5.1c). Hatun [53] and Marsh [3] showed that the increasing temperature and salinity in the SPG in the late 1990s was related to the increased convergence of the Atlantic Current Waters in the sup-polar ocean. This process, which is well reproduced by my model was related to weakening of the SPG [53](see Fig. 5.1a).

The volume flux of the flow through the Southern Sub-polar section (Fig. 5.2a) was lowest in the 1980s and highest in the 2000s. The decadal average of the volume flux increased from 40Sv to 42Sv between the 1990s and 2000s. The temperature of the Southern Sub-polar section (Fig. 5.2b) did not increase steadily, instead it increased in jumps between the 1970s and 1980s and between the 1990s and 2000s. The decadel mean temperature increased by about 0.8°C during the study period. The salinity of the Southern Sub-polar section (Fig. 5.2c) follows a similar trend as the temperature with a mean decadal increase of about 0.03PSU during the study period. The volume flux, temperature and salinity all experienced a decrease during 1985-1995.

The decadal average temperature and salinity of the two sections closely resemble each other (see Fig. 5.1b, 5.1c,5.2b,5.2c).

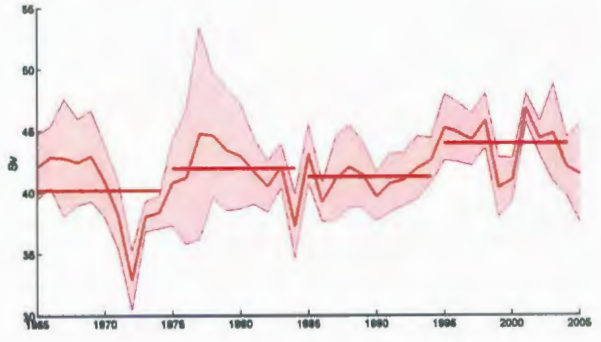

a Volume Flux

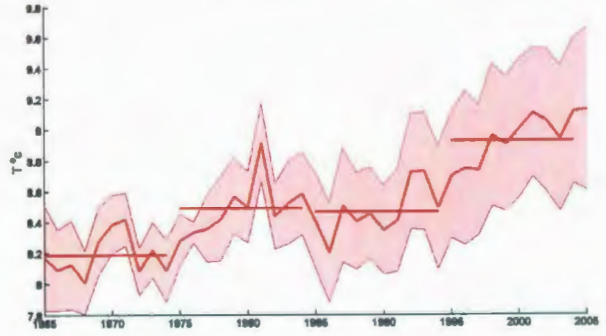

b Temperature

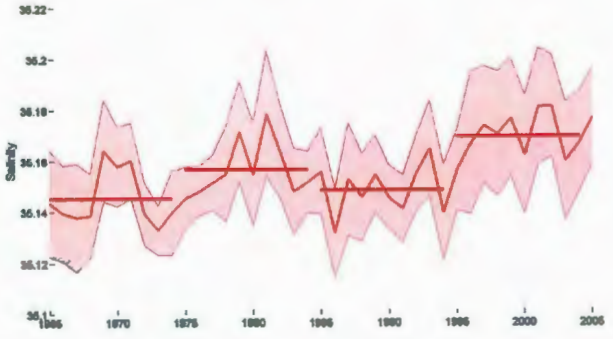

c Salinity

Figure 5.2: Varability of (a) total volume flux , (b) temperature and (c) salinity in the Southern Sub-polar section.

5.2 Variability of the Nordic Straits

The flow through the three sections, the Greenland-Scotland Ridge, the Barents Sea Opening and the Fram Strait have different properties and are studied separately, see Fig. 4.1. While the transport in the sub-polar ocean showed a strong interannual variability the flow over the Greenland-Scotland Ridge was less variable (see Fig. 5.3a). There was a steady increasing trend in the decadal mean volume flux since 1985. The temperature of the water flowing over the Greenland-Scotland Ridge (see Fig. 5.3b) closely follows the variability of the temperature in the sub-polar ocean (see Fig. 5.9). Apart from the quasi-decadal oscillation of 1977-1987 there is little variability of the salinity of the Greenland-Scotland Ridge (figure 5.3c).

The volume flux of the Barents Sea Opening (BSO) is small (a magnitude of about 0.6Sv) when compared with the other straits (a magnitude of about 3Sv in the Greenland-Scotland Ridge for example). The BSO also experiences decadal variability in the volume flux (Fig. 5.4a). The mean decadal temperature of the BSO has an increasing trend for the entire study period,(Fig. 5.4b), while the salinity is quasi-constant for the entire study period (Fig. 5.4c).

The variability of the transport through the Fram Strait is greater than that through the BSO (Fig. 5.5a). The maximum of the decadal mean of the transport occurred during 1985-1995 (Fig. 5.5a), unlike the Greenland-Scotland Ridge which occurred during 1995-2005 (Fig. 5.3a). Both the temperature and salinity decadal means through the Fram Strait experienced increasing trends with increases of 0.2^{o}C and 0.5PSU respectively.

The temperature and salinity of the water masses of the Nordic Seas vary dif-

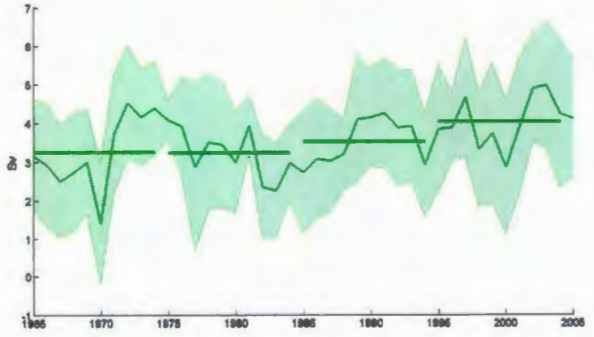

a Volume flux

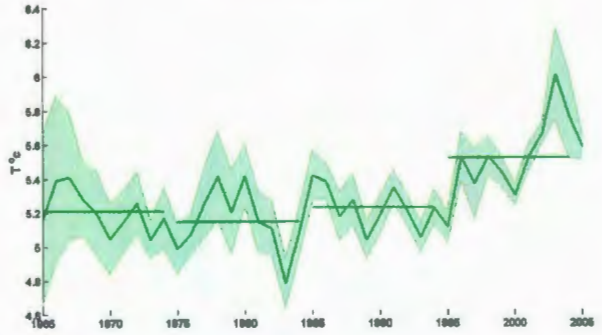

b Temperature

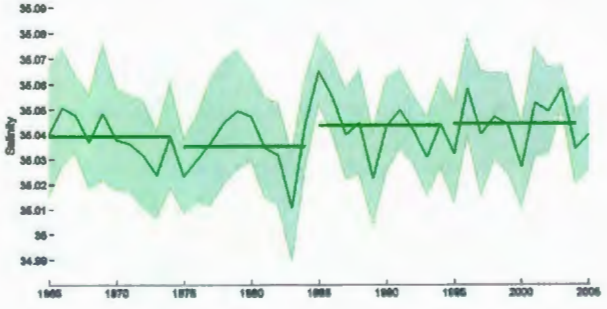

c Salinity

Figure 5.3: Varability of (a) total volume flux , (b) temperature and (c) salinity over the Greenland-Scotland Ridge.

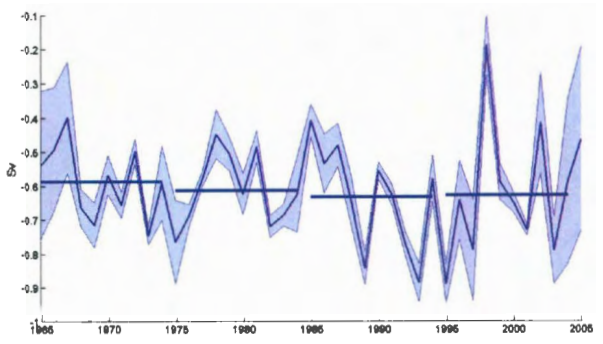

a Volume flux

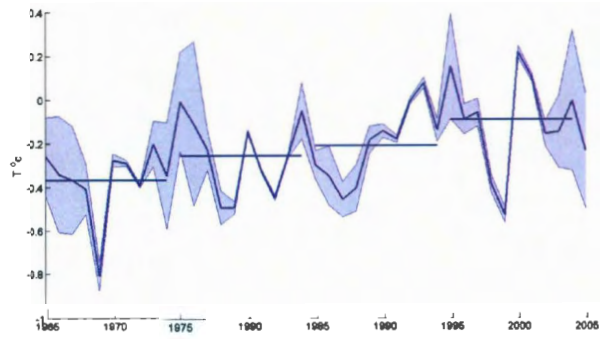

b Temperature

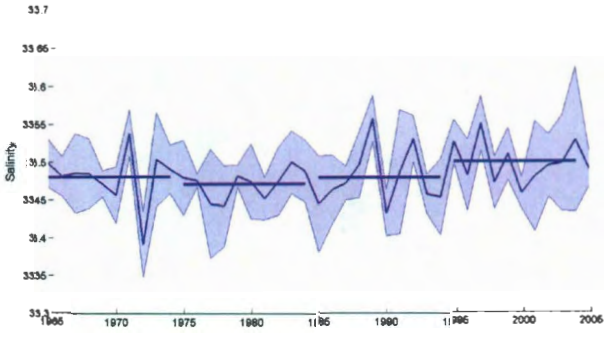

c Salinity

Figure 5.4: Varability of (a)total volume flux , (b) temperature and (c) salinity in the Barents Sea Opening

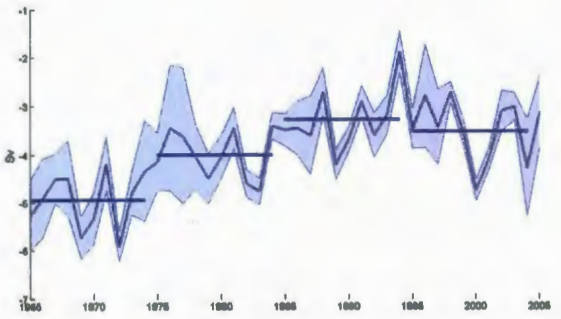

a Volume Flux

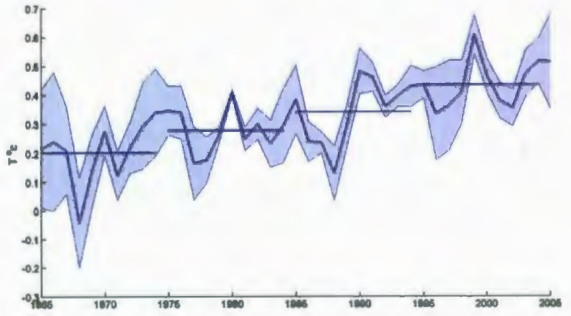

b Temperature

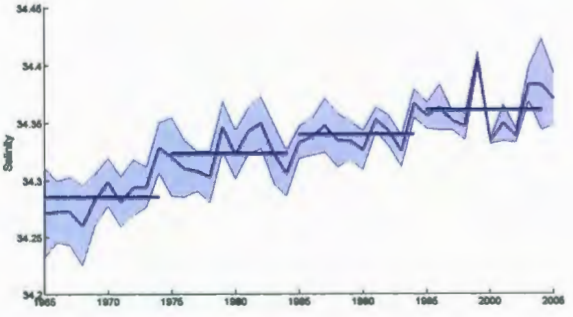

c Salinity

Figure 5.5: Varability of (a) volume flux , (b) temperature and (c) salinity in the Fram Strait

ferently. Figs. 5.6a and 5.6b show the variability of the Atlantic water that crosses the Greenland-Scotland Ridge and Fram Strait and Figs. 5.7a and 5.7b shows the polar water. The definitions of the water masses are given in the figure caption. Peaks, both negative and positive, in the temperature and salinity of the AW across the Greenland-Scotland Ridge and the Fram Strait occur in the late 1980s and early 1990s (see Fig. 5.6a and 5.6b). Across the Greenland-Scotland Ridge the AW's salinity and temperature normalized anomalies had different magnitudes in 1965-1975 and 1995-2005. This is during times of consistent NAO and not during transition between the two phases of NAO. The mechanism of this difference is beyond the scope of this work. There is little interannual variation of the polar water in the Fram Strait except for a large lone peak in 1985. There is also no variation on the decadal mean of the Fram's polar water salinity and temperature.

5.3 Heat Balance of Sub-Polar and Nordic Seas

The variability in the volume flux, temperature and salinity in all the straits has an effect on the heat and salt balance in the Sub-polar region and the Nordic Seas. The flow over the ridge not only carries mass (volume) it also transports heat and salt. The heat flux is estimated using

$$H(t) = \int_A c_p \rho V_A(t) T(t) dA \tag{5.1}$$

where c_p is the heat capacity of seawater, ρ is the density. $H(t)$ is the heat flux for an area and $V_A(t)$ and $T(t)$ are the volume flux and temperature. In order for this heat flux to have any physical meaning it should be independent to the choice of

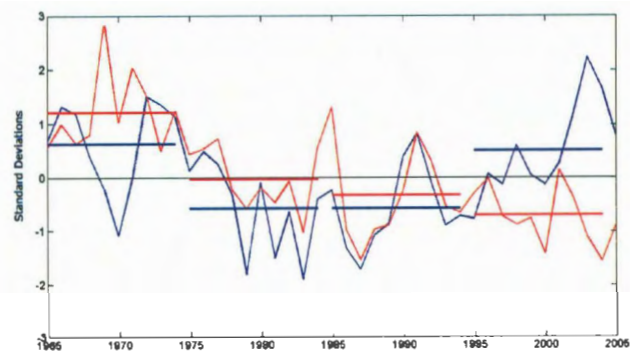

a Greenland Scotland Ridge AW

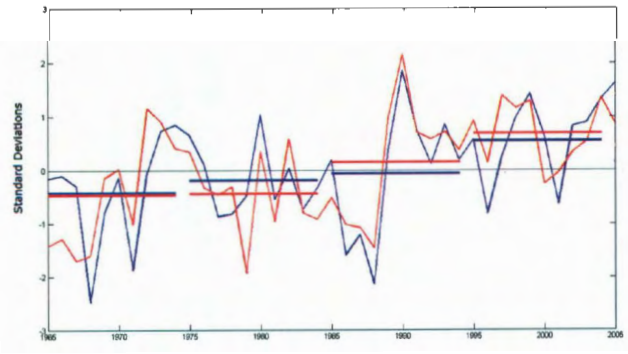

b Fram Strait AW

Figure 5.6: Varability of the Atlantic water mass passing through the straits of the Nordic Seas. In all parts the normalized anomaly of the temperature is given in blue and the normalized anomaly of the salinity is red. (a) The variability of the Greenland-Scotland Ridge AW (S>=35 and T>6). (b) The variability of the Fram Strait AW (S>34.5 and T>1).

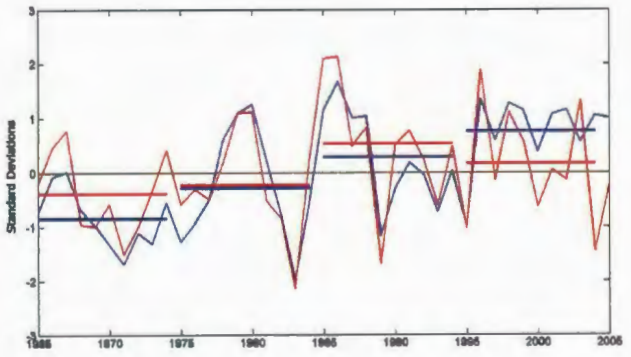

a Greenland Scotland Ridge PW

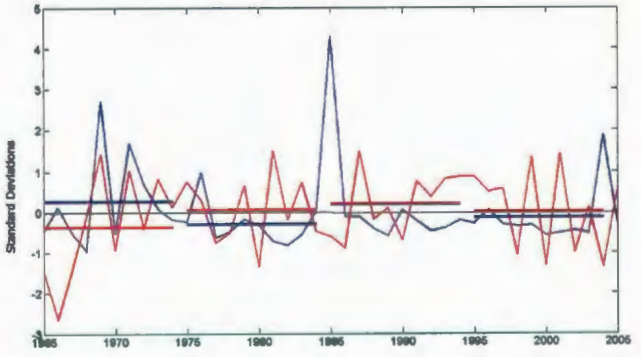

b Fram Strait AW

Figure 5.7: Varability of the polar water mass passing through the straits of the Nordic Seas. In all parts the normalized anomaly of the temperature is given in blue and the normalized anomaly of the salinity is red. (c) The variability of the Greenland-Scotland Ridge polar water (S< 35 and T< 3). and (d) The variability of the Fram Strait polar water (S< 33 and T< -0.5).

temperature scaled used. For example the heat flux calculated using Celsius should equal the heat flux calculated using Kelvins. However, because $T_K = T_{\circ C} + 273$ we get the different heat fluxes using T_k and $T_{\circ C}$:

$$\begin{aligned} H_K &= \int_A c_p \rho V_A(t) T_K(t) dA \\ H_{\circ C} &= \int_A c_p \rho V_A(t) T_{\circ C}(t) dA + 273 \int_A c_p \rho V_A(t) dA \end{aligned} \tag{5.2}$$

If the flow through the strait is balanced then $\int_A V_A(t) dA = 0$, then $H_{\circ C}$ and $H_{\circ K}$ would be the same. The sum of the volume flux through each of the Greenland-Scotland Ridge, Fram Strait and BSO does not vanish. They are balanced by and therefore equal to the flux through the Bering Strait. This uncertainty is not present if we calculate the total heat flux into a closed region, where $\oint_A V_A(t) dA = 0$. The annual mean flow is quasi-non-divergent and hence the heat flux is independent of the temperature scale used.

The net heat flux here is calculated for the Nordic and Sub-Polar Seas separately. The lateral oceanic heat fluxes into the Sub-polar sea and Nordic Seas are calculated using equation 5.1 across 3 separate sections for each sea and then added together with the atmospheric heat flux. The total heat flux into a region is equal to change in the heat content of that region. The total heat flux,$H(t)$, is proportional to the change in the average temperature of that region, shown in the equation below.

$$H(t) = \frac{\Delta heatcontent}{\Delta t} \approx \frac{c_p \rho V \Delta T}{\Delta t} \propto \frac{\Delta T}{\Delta t} \tag{5.3}$$

The highest values in the heat flux $H(t)$ correspond to the steepest increase of the temperature in time. Peaks in the heat flux result in a rapid positive trend in

the temperature. The temperature is also increased as a result of a long term small positive anomaly in the heat flux.

The decadal mean of the total heat flux into both the Nordic and Sub-Polar Seas is highest for the entire study period in 1995-2005 (Fig. 5.8 and Fig.5.10) . For the Sub-Polar Sea there was a statically significant ($p<0.025$) decrease in the total heat flux in the 1990s (Fig. 5.8) while in the Nordic Seas the the heat flux decadal mean increased steadily (Fig. 5.10). From Fig.5.8 and Fig.5.10 it can be seen that there was a large increases in the decadal mean of the heat flux in the Sub-Polar Sea between the 1985-1995 and 1995-2005 and an increase from a negative anomaly to a positive anomaly of heat flux between the decades 1975-1985 and 1985-1995.

There is a large statically significant ($p<0.01$) increase in the temperature between 1985-1995 and 1995-2005 in the Sub-Polar Sea, as seen in Fig. 5.9. This corresponds to the peaks in the heat balance 1997 and 2003 as well as with the positive decadal anomaly of the heat flux during that time, Fig. 5.8. This result corresponds to findings of Marsh et al [3].

Figures 5.10 and 5.11 show that in the Nordic Seas the temperature anomaly was positive from 1990-2005 and was strongly negative from 1965-1990 while the heat flux was positive from 1985-2005 and oscillated between positive and negative for 1965-1990. The very high peaks in the heat flux in the 1970s and in the early 1990s lead to a rapid increase in the temperature in the Nordic Seas. However, after 1990 there were no strong peaks in the heat flux anomaly but the temperature was the warmest for the entire study period. Therefore the, statically significant ($p<0.025$), increase in the temperature between 1995 and 2005 is a result of small, but long standing,

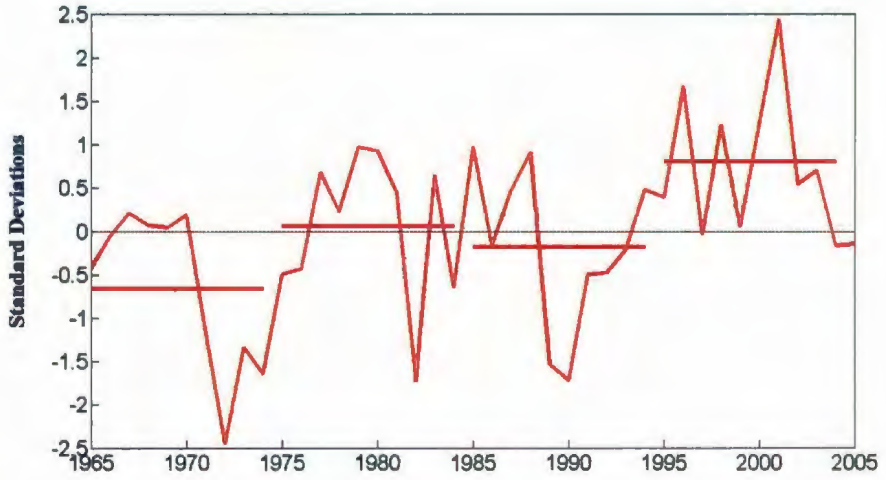

Figure 5.8: Anomaly of the net heat flux into the Sub-Polar Sea. (The flux is normalized by its standard deviation.)

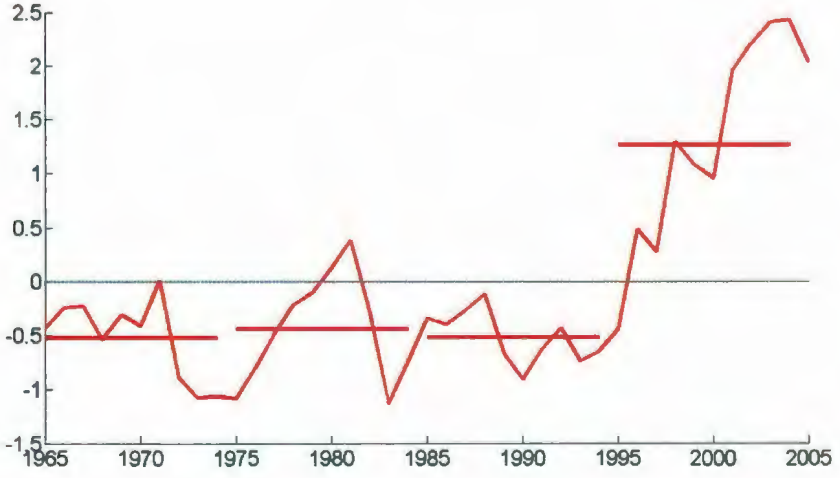

Figure 5.9: Anomaly of the average temperature of the Sub-Polar Sea(normalized by its standard deviation.)

positive anomaly in the total heat flux.

5.4 On the mechanism of decadal variability of the Atlantic Water in the Nordic Seas

The NAO plays a major role for the climate of the sub-polar and Nordic Seas. In 1965-1980 the NAO index was predominantly negative. Between the 1980s and the 1990s the NAO index changed in to a positive phase. During the 1990s there was a large increase in the NAO index, and during 2000-2005 the NAO decreased while still remaining positive (Fig. 2.7c).

The volume transports shown in the previous two sections are calculated as a mean over the area of the straits. Thus, they show the balance between the northward flow of AW and the southward flow of cold surface polar water. Fig. 5.12 show these two fluxes separately for the Greenland-Scotland Ridge, the Fram Strait and the BSO. The fluxes in and out of the Nordic Seas balance each other in order to maintain the long term mass balance of the basin. However, at the same time these fluxes show interannual variability which influences the heat and salt balance of the basin.

When comparing the inflow into the Nordic Seas over the Greenland-Scotland Ridge with the outflow through the Fram Strait and the Barents Sea Opening, Fig. 5.12, we can see that there is a mismatch in the change in the inflow for the late 1980s to the late 1990s. During this period of time there is more warm water entering the Nordic Seas than leaving through the Fram Strait and Barents Sea Opening and this results in more of the Atlantic water recirculating in the Nordic Sea. This

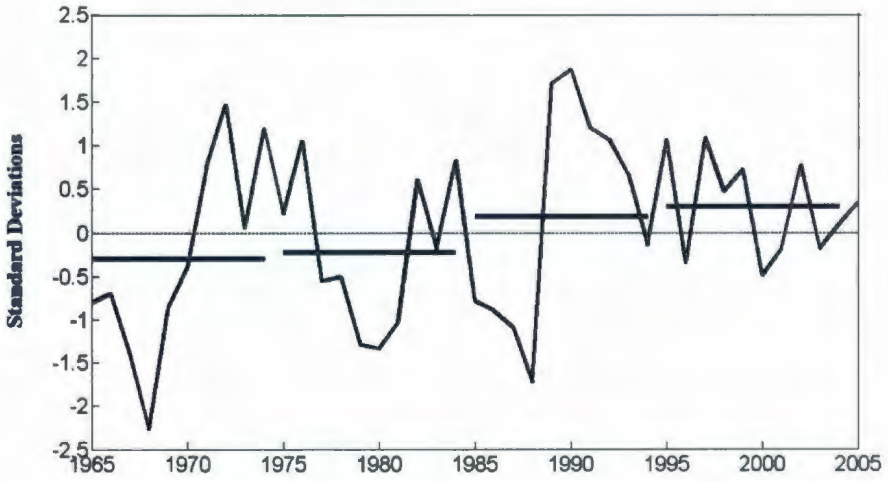

Figure 5.10: Anomaly of the net heat flux into the Nordic Sea (normalized by its standard deviation.)

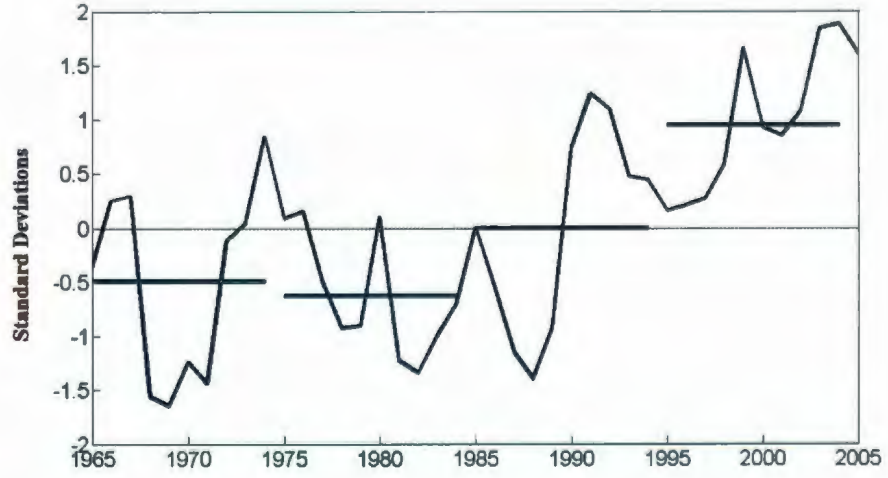

Figure 5.11: Anomaly of the average temperature of the Nordic Sea (normalized by its standard deviation.)

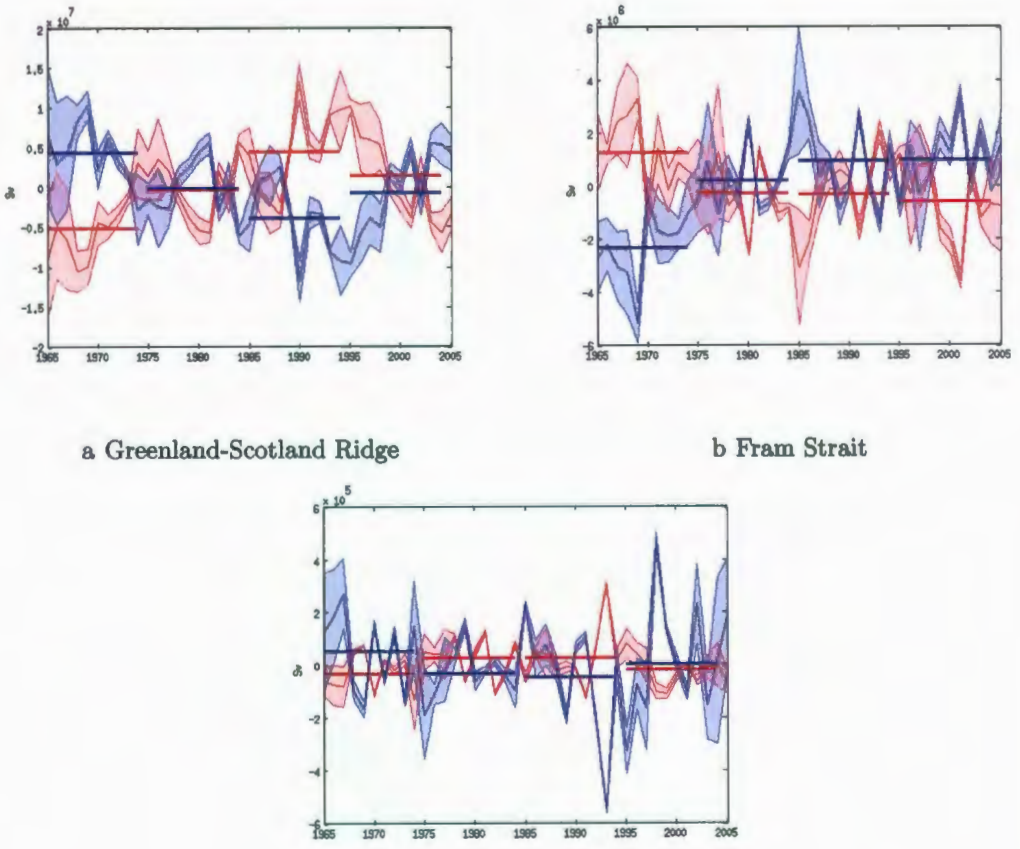

a Greenland-Scotland Ridge

b Fram Strait

c BSO

Figure 5.12: Northward (red) and Southward (blue) volume fluxes over the (a) Greenland-Scotland Ridge, (b) through the Fram Strait and (c) through the Barents Sea Opening.

recirculating Atlantic water causes a build up of warm water in the Nordic Seas and therefore an increase in the average temperature during this period, (see Fig. 5.11). The intensified inflow of AW through the Greenland-Scotland Ridge correlates well with the positive NAO index, which is known to be the dominant factor for intensified transport in the sup-polar ocean (Fig 5.1a).

In the late 1990s the flow mismatch no longer exists due to a lowering of the NAO index and decay of the SPG after 1995. However the temperature of the Nordic Seas continued to increase after 1995. While the transport is lower than normal an increase in the temperature of the water in the Sub-polar Sea during that time (Fig. 5.9), caused an increase in the temperature of the water mass that crosses the Greenland-Scotland Ridge, (Fig. 5.3b).

Figures 5.13 and 5.14 shows the lagged correlation between the maximum temperature of the water column and the maximum temperature of the water through the Fram Strait(lagged). It is calculated over two periods, 1965-1985 (Fig. 5.13) and 1985-2005 (Fig. 5.14). Figure 5.13 shows the positive correlation of AW flowing into the Nordic Seas with the AW temperature at the Fram Strait. It clearly shows the propagation of the core of the AW along two parts. The first part is the recirculation path in the Nordic Seas and the second path is through the BSO and towards Novaya Zemlya Island. The time scale of the spreading in the Nordic Seas is about 4 years. In 1965-1985 the first path is much weaker than in 1985-2005. As mentioned above the recirculation during this time, 1965-1985, was weaker and therefore is more difficult to identify in the temperature lag correlation map.

The temperature of the Nordic Seas (Fig. 5.3b) started increasing in 1980s. In

1985-1995 the temperature increase in the Nordic Seas correlates to the inflow/outflow mismatch which led to more Atlantic water recirculating and therefore a build up of warm water. This is confirmed by the correlation maps. In 1995-2005 the temperature increase in the Nordic Seas is related to the increase in the temperature of the inflow from the sub-polar, as the sub-polar experienced a dramatic warming between 1995-2005.

5.5 Impact of heat and volume fluxes on the Arctic Ocean variability.

The warming in the Nordic Seas in the 1980s and 1990s influenced the properties of the water flowing into the Arctic Ocean. Following Polyakov et.al.[55] the Atlantic water core temperature (AWCT) is defined as the maximum temperature of the water column greater than 0°C. The AWCT in the model results was calculated and compared with the observations of Polyakov. As seen in Fig. 5.15 the long term variability in the AWCT in both model results and observations is a steady negative normalized anomaly from 1965-1985. An increasing trend into the positive anomaly is present for 1985-2005, when warming occurred in the Nordic Seas.

The depth of the AWCT also showed a strong interannual variability (see Fig.5.16). The core depth is steady between 1975-2005 except for a large decrease in the depth in 1990.This dip in the core depth occurs at the same time as the shift to extra recirculation in the Nordic Seas.

There was also a shift in the bottom water of the Arctic Ocean. The bottom

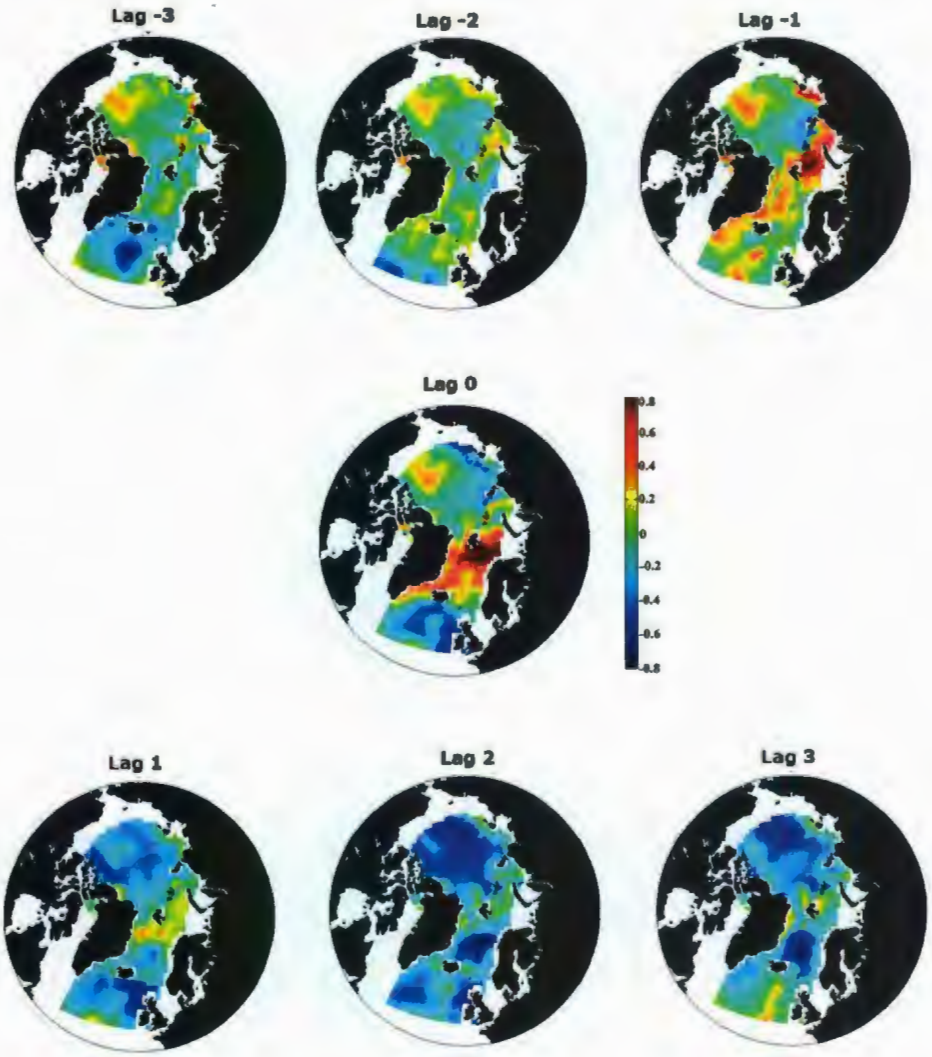

Figure 5.13: Lagged correlation between maximum temperature of water column and water in Fram Strait for 1965-1985

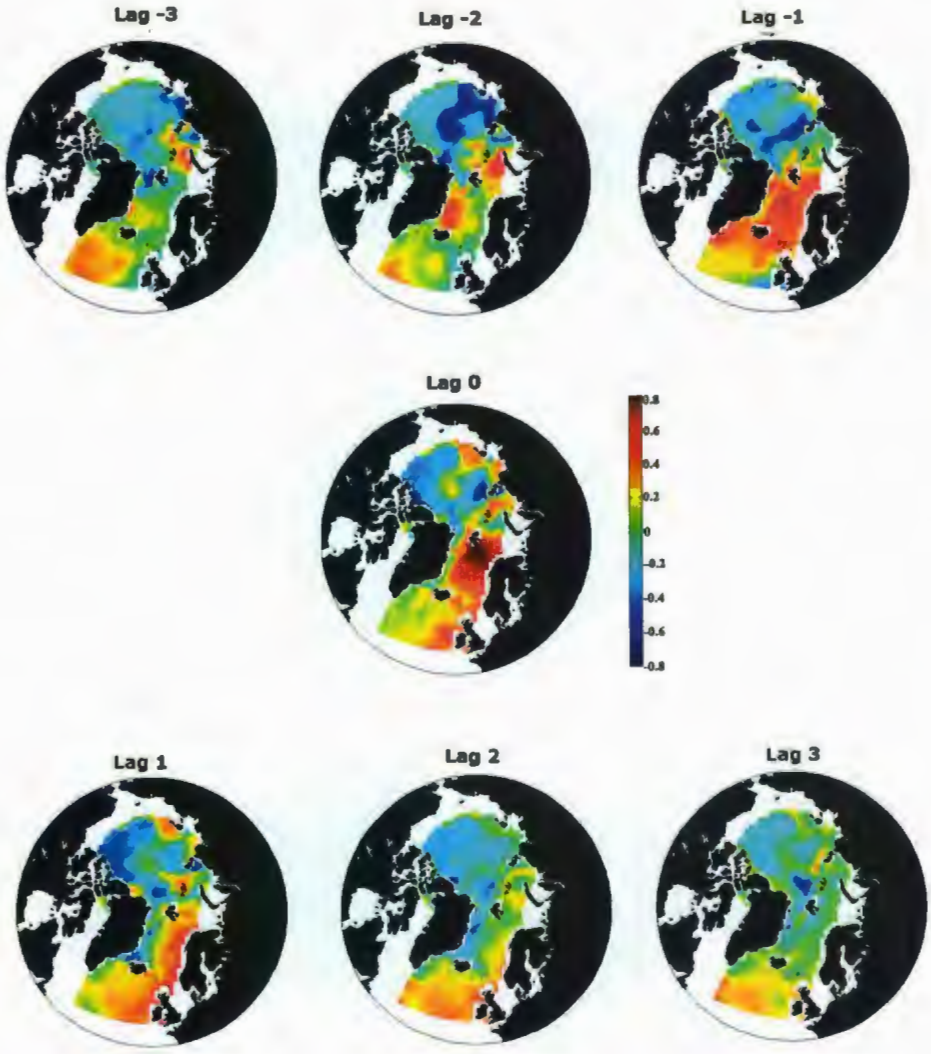

Figure 5.14: Lagged correlation between maximum temperature of water column and water in Fram Strait for 1985-2005

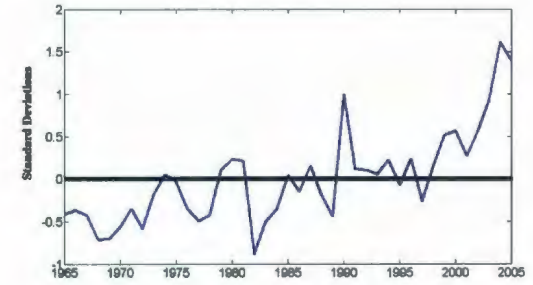

a Model

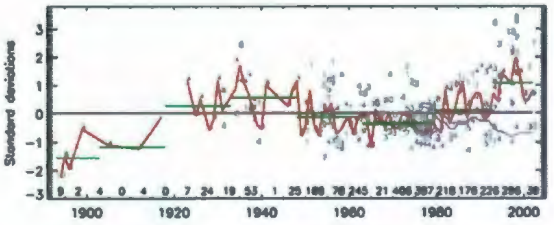

b Observations

Figure 5.15: Normalized anomaly of the Atlantic Water Core Temperature in the Arctic Ocean from (a) Model results and (b) Observations [55].

water core temperature (BWCT) of the Arctic Ocean is defined as the coldest water at every point in the Arctic Ocean below the surface layer. The BWCT shown in Fig.5.17 is calculated as the meridional mean of the BWCT from 80°N to 90°N.The mean BWCT at 0°E, which is where the Atlantic water enters the Arctic Ocean, is anomalously cold before 1990 and anomalously warm after. At 180°E, where the Pacific water enters the Arctic ocean the mean BWCT is anomalously warm before 1990 and anomalously cold after. This is seen in Fig. 5.17.

The BWCT near 0°E, where the the Atlantic water enters the Arctic Ocean, has a very strong correlation ($r = 0.5568$, $p<0.001$) to the temperature of the Nordic Seas. The negative anomalies of the average Nordic Seas temperature, (see Fig. 5.11)

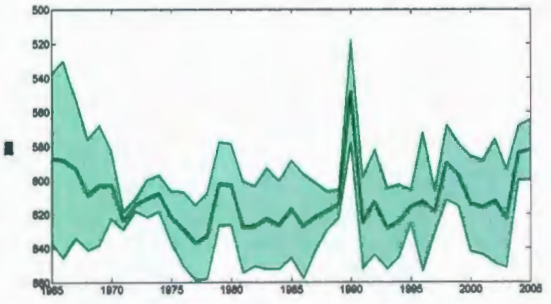

Figure 5.16: Depth of the AWCT in the Arctic Ocean

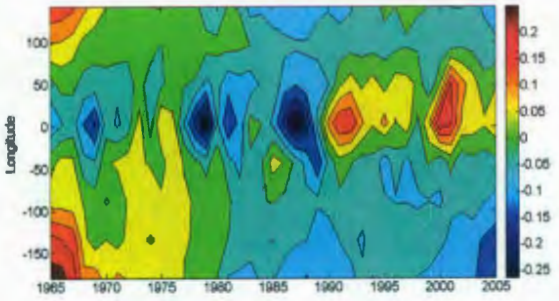

Figure 5.17: Normalized Anomaly of Bottom water core temperature

in 1968, 1979,1981 and 1987 corresponds to the minimum BWCT at this location. Similarly, the positive anomalies in 1973-1976, 1985, 1992, 1998,and 2003 in the Nordic Seas temperature corresponds to the high temperatures of the BWCT at 0°E.

This variability in the AWCT as well as the variability of the seaice is affected by Cold Halocline Layer (CHL). The CHL's strong salinification prevents convection between the surface layers and the AW layer. Therefore, as the strength of the CHL varies so does the communication between the surface layers and the deeper waters. The CHL varies in coverage and strength [56, 57]. However, the model used in this study has a vertical and horizontal resolution that is too coarse to properly resolve

the CHL and therefore the CHL will not be discussed with respect to the variability in this thesis.

Variability of the AW that enters Arctic Ocean is just one of many ways in which the ocean can be warmed. It is also warmed by changes in atmospheric heat fluxes over the Arctic, reduction/increase of sea ice (its thermal and momentum barrier) and by variability of Pacific water transport through the Bering Strait. Warming may also be caused by internal restructuring of the ocean. Changes in thermo- and haloclines may reduce or increase the communication of certain water masses with the atmosphere where the majority of heat is lost which in turn would cause the ocean to warm or cool. However, the lateral variability of heat flux is greater than the atmosphere-ocean heat fluxes and the temperature and salinity anomalies in the Arctic Ocean are associated with the hydrographic anomalies of the same sign in the Nordic Seas [55].

Chapter 6

Summary and Conclusions

6.1 Summary

Over the last two decade many changes have been observed in the Sub-polar sea, Nordic seas and the Arctic Ocean. The temperature at the surface and at depth have increased and this has lead to a decrease in sea ice and to an increase in the discharge rate of glaciers of the Greenland Ice-sheet. This melting of sea ice and increase in glacier discharge potentially has large global impacts. Understanding the mechanisms of the warming in the Nordic Seas and Arctic Ocean and its variability are important for understanding the Earth's climate.

Using a 2^o resolution model the variability of the Arctic Ocean and Nordic Seas has been studied. All of the straits of the Nordic Seas experience interannual and decadal variability in their volume flux, temperature and salinity. There was an increase in the temperature of the water entering the sub-polar section from the northern North Atlantic and the water crossing the Greenland-Scotland Ridge northward for

the period 1995-2005. The decadal mean temperature through the Fram Strait and the Barents Sea Opening monotonically increased between 1965 and 2005. So, the increase seen in the temperature to the south was not directly related to the variability in the straits to the north.

The decadal mean of the salinity through all the Nordic straits increased monotonically except through the Southern Sub-polar section which experienced a large jump between the 1980s and the 1990s. The volume flux through the southern sub-polar section and over the Greenland-Scotland Ridge increased steadily between 1965 and 2005 while the volume flux through the Barents Sea Opening remained almost constant and the volume flux through the Fram Strait increased until 1995 where it then decreased slightly.

There was also an increase in the average temperature of the Sub-polar and Nordic seas during the last decade of almost 2°C in the Sub-polar Sea and 1°C in the Nordic Seas. The warming started in the Sub-polar seas in the mid-1990s while the warming started downstream earlier in the Nordic Seas in late 1980s and 1990s. The decadal mean of the heat flux into the Nordic Seas increased steadily until 1995 where it increased to higher values.

The lateral heat fluxes into the region are greater than that of the surface heat fluxes. The variability of the heat flux into a region is therefore related to the variability of the average temperature of that region. Large peaks in the heat flux into a region and long term positive anomalies in the heat flux both result in an increase in the temperature. After 1995 the temperature increase in the Sub-polar section and the Nordic Seas is a result of long term positive anomaly in the heat flux into the

region which is a result of the increase in the temperature of the water entering into the region.

The temperature variability in the Nordic Seas affected the temperature of the Arctic Ocean. The decadal mean warming in the Nordic Seas corresponds to the warming in the Atlantic water layer after 1985. The interannual variability of the Nordic Seas temperature affected the bottom water core temperature of the Arctic Ocean.

6.2 Interpretation of Findings

The period 1985-1995 was a period of very high positive NAO index. Our model simulations confirm the results of previous studies that the temperature of the sub-polar ocean decreased during that time [58] and the intensity of the SPG increased. The NAO after 1995 decreased while remaining in the positive phase. The temperature of the sub-polar ocean was higher than normal during this time. In the Nordic Seas the flow of Atlantic Water over the Greenland-Scotland Ridge increased between 1985 and 1995. The flow of AW through the Fram Strait did not increase during this time. This resulted in a flow imbalance of warm AW and consequently warming of the Nordic Seas. After 1995, when the NAO decreased its strength, the flow of AW over the Greenland-Scotland Ridge slowed and so ended the flow mismatch. The AW entering the Nordic Seas in this period was warmer than normal and this maintained the positive heat flux into the region. The warming of the Arctic Ocean in the model simulations is a response to the warm inflow from the Nordic Seas.

Chapter 7

Future Work

The present study of the Arctic and Sub-Arctic oceans can be extended towards future climate projections of this region. Using the IPCC climate scenarios as the atmospheric forcing for our model future projections can be made.

This ocean model was applied in preliminary simulations in the Arctic. However, when using the model for future scenarios no spectral nudging was applied because there are no observations to force the results towards. The first results show that there is a very large decrease in sea ice cover from 2000 to 2100 for both summer and winter with the most noticeable being the summer (Fig. 7.1). In the winter the sea ice retreats to about 2/3 of its original size. Hudson's Bay loses almost all of its ice and the Bering Strait is open in winter 2100. There is no sea ice in the winter along the east coast of Greenland in 2100 which can have detrimental effects on the stability of the Greenland Ice Sheet. In the summer there is almost a complete loss of sea ice cover in the Arctic by 2100. This will be a major problem for the wildlife in the region such as polar bears and seals which depend on the sea ice. Associated

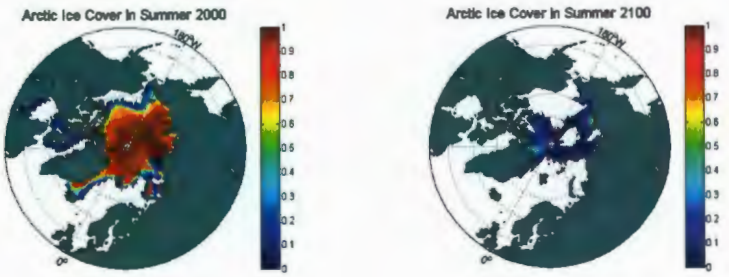

a Summer 2000 b Summer 2100

Figure 7.1: Ice cover in Summer for (a) 2000 and (b) 2100.

with loss of sea ice is warming of the waters of the Arctic Ocean. There is a general warming trend in the top 1000m between 2000 and 2100. This is especially evident for 50 to 150°E where the increase in temperature is on the order of 3°C. This is where the AW enters the Arctic Ocean (Fig. 7.2).

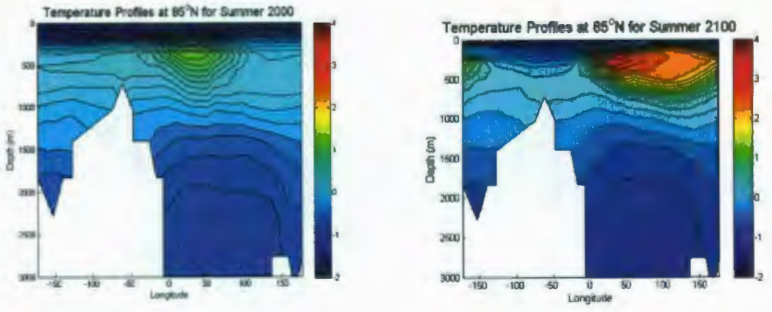

a Temperature 2000 b Temperature 2100

Figure 7.2: Depth Profile of Temperature in °C in Summer for (a) 2000 and (b) 2100.

The preliminary results demonstrate some confidence in the present model's ability to provide a good basis for simulations of regional projections through local refinement of the model grid and by coupling that model with an atmospheric model.

Bibliography

[1] P. Lemke, J. Ren, R.B. Alley, I. Allison, J. Carrasco, G. Flato, Y. Fujii, G. Kaser, P. Mote, R.H. Thomas, and T. Zhang. Observations:changes in snow, ice and frozen ground. In S. Solomon, D. Qin, M. Manning, Z. Chen, M. Marquis, K.B. Averyt, M. Tignor, and H.L. Miller, editors, *Climate Change 2007: The Physical Science Basis. Contribution of Working Group I to the Fourth Assessment Report of the Intergovernmental Panel on Climate Change*. Cambridge University Press, Cambridge, United Kingdom and New York, NY, USA, 2007.

[2] D. McBean, G. Alekseev, D. Chen, E. Forland, J. Fyfe, P.Y. Groisman, R. King, H. Melling, R. Vose, and P.H. Whitfield. *Arctic Climate Impact Assessment*, chapter Arctic Climate: Past and Present. Cambridge University Press, 2005.

[3] R. Marsh, S. A. Josey, B.A. de Cuevas, L.J. Redbourn, and G.D. Quartly. Mechanisms for recent warming of the north atlantic: Insights gained with an eddy-permitting model. *Journal of Geophysical Research,*, 113, 2008.

[4] D.M. Holland, R.H. Thomas, B. De Young, M.H. Ribergaard, and B. Lyberth. Acceleration of jakobshavn isbrae triggered by warm subsurface ocean waters. *Nature Letters*, 2008.

[5] T.Vinje. Anomalies and trends of sea-ice extent and atmospheric circulation in the nordic seas during the period 1864-1998. *American Meteorological Society*, 2000.

[6] K. Mork and J. Blindheim. Variations in the atlantic inflow to the nordic seas. *Deep-Sea Research I*, 47:1035–1057, 2000.

[7] K.Lohmann, H.Drange, and M.Bentsen. Response of the north atlantic subpolar gyre to persistent north atlantic oscillation like forcing. *Clim Dyn*, 32:273–285, 2008.

[8] B. Hansen, S. Osterhus, W. R. Turrell, S. Jonsson, H. Valdimarsson, H. Hatun, and S. M. Olsen. *Arctic-Subarctic Ocean Fluxes - Defining the role of the northern seas in climate*, chapter The Inflow of Atlantic Water, Heat and Salt to the Nordic Seas. Springer, 2008.

[9] B.Hansen, W.R.Turrell, and S.Osterhus. Decreasing overflow from the nordic seas into the atlantic ocean through the faroe bank channel since 1950. *Nature*, 411:927–930, 2001.

[10] O Skagseth, T. Furevik, R. Ingvaldsen, H. Loeng, K. A. Mork, K. A. Orvik, and V. Ozhigin. *Arctic-Subarctic Ocean Fluxes - Defining the role of the northern seas in climate*, chapter Volume and Heat Transports to the Arctic Ocean. Springer, 2008.

[11] U. Schauer, A. Beszczynska-Moller, W. Walczowski, E. Fahrbach, J. Piechura, and E. Hansen. *Arctic-Subarctic Ocean Fluxes - Defining the role of the northern*

seas in climate, chapter Variation of Measured Heat Flow Through the Fram Strait Between 1997 and 2006. Springer, 2008.

[12] M.Karcher, R.Gerdes, and F.Kauker. *Arctic-Subarctic Ocean Fluxes - Defining the role of the northern seas in climate*, chapter Long-Term Variability of Atlantic Water Inflow to the Northern Seas: Insights from Model Experiments. Springer, 2008.

[13] T.D. Prowse and P.O. Flegg. *The Freshwater Budget of the Arctic Ocean*, chapter Arctic River Flow: A review of contributing areas. Kluwer Academic Publishers, 1998.

[14] L. Rey. *The Arctic Ocean: The Hydrographic Environment and the Fate of Pollutants*, chapter The Arctic Ocean: A 'Polar Mediterranean'. Wiley-Interscience Publications, 1982.

[15] H. Haak, J. Jungclaus, U. Mikolajewicz, and M. Latif. Formation and propagation of great salinity anomalies. *Geophysical Research Letters*, 30(9), 2003.

[16] G. Bjork, M. Jakobsson, B. Rudels, J. H. Swift, L. Anderson, D. A. Darby, J. Backman, B. Coakley, P. Winsor, L. Polyak, and M. Edwards. Bathymetry and deep-water exchange across the central lomonosov ridge at 88-89.1 n. *Deep-Sea Research I*, 54:1197–1208, 2007.

[17] J. Blindheim and S. Osterhus. The nordic seas, main oceanographic features. In *The Nordic Seas: An Integrated Perspective.*, volume AGU Monograph 158, Washington DC, 2005. American Geophysical Union.

[18] B. Hansen and S. Osterhus. North atlantic - nordic seas exchanges. *Progress in Oceanography*, 45:109–208, 2000.

[19] J. L. Murray. *AMAP Assessment Report: Arctic Pollution Issues*, chapter Physical/Geographical Characteristics of the Arctic. Arctic Monitoring and Assessment Programme (AMAP), 1998.

[20] G. Madec. *NEMO ocean engine - version 3.1* -. Laboratoire d'Oceanographie et du Climat: Experimentation et Approches Numeriques, 2008.

[21] R. Przybylak. *The climate of the Arctic.* Springer, 2004.

[22] National Snow and Ice Data Center. Education center-arctic climatology and meteorology. http://nsidc.org/arcticmet/.

[23] N. Steiner, G. Holloway, and T. Sou. Estimation of arctic windspeeds and stresses with impacts on ocean-ice snow modeling. *Journal of Marine Systems*, 39:129 –151, 2003.

[24] D. J. Gregor, H. Loeng, and L. Barrie. *AMAP Assessment Report: Arctic Pollution Issues*, chapter The Influence of Physical and Chemical Processes on Contaminant Transport into and within the Arctic. Arctic Monitoring and Assessment Programme (AMAP), 1998.

[25] J. A. Bradbury and C. P. Wake. Airmap: Atmospheric investigation, regional modeling, analysis and prediction climate change research center. http://airmap.unh.edu/background/nao.html University of New Hampshire Earth Sciences, 2004.

[26] Nao index data provided by the climate analysis section, ncar, boulder, usa, hurrell (1995).

[27] R.Dickson, T.Osborn, J. Hurrell, J. Meincke, J. Blindheim, B. Adlandsvik, T. Vinje, G. Alekseev, and W. Maslowski. The arctic ocean response to the north atlantic oscillation. *Journal of Climate*, 13:2671–2696, 2000.

[28] J. Bjerknes. Atlantic air-sea interaction. *Adv Geophys*, 10:1–82, 1964.

[29] J.E. Overland and M. Wang. The arctic climate paradox: The recent decrease of the arctic oscillation. *Geophys. Res. Lett.*, 32, 2005.

[30] B. Wu, J. Wang, and J.E. Walsh. Dipole anomaly in the winter arctic atmosphere and its association with sea ice motion. *J. Climate*, 2006.

[31] J. Maslanik, S. Drobot, C. Fowler, W. Emery, and R. Barry. On the arctic climate paradox and the continuing role of atmospheric circulation in affecting sea ice condtions. *Geophys. Res. Lett.*, 2007.

[32] J. Wang, J. Zhang, E. Watanabe, M. Ikeda, K. Mizabata, J.E. Walsh, X. Bai, and B. Wu. Is the dipole anomaly a major driver to record lows in arctic summer sea ice extent? *Geo. Phy. Res. Lett.*, 2009.

[33] M. Ambaum, B.Hoskins, and D. Stephenson. Arctic oscillation or north atlantic oscillation? *Journal of Climate*, 14:3495–3507, 2001.

[34] J. Cohen and M. Barlow. The nao, the ao and global warming: How closely related? *Journal of Climate*, 18:4498–4513, 2005.

[35] L.k. Coachman and K. Aagaard. *Marine Geology and Oceanography of the Arctic Seas*, chapter Physical Oceanography of Arctic and Subarctic Seas. Springer-Verlag, 1974.

[36] I.E. Frolov, Z.M. Gudkovich, V.F. Radionov, A.V. Shirochkov, and L.A. Timokhov. *The Arctic Basin: Results from the Russian Drifting Stations.* Springer-Praxis, St.Petersburg, Russia, 2005.

[37] R.D. Muench, M.G. McPhee, C.A. Paulson, and J.H. Morrison. Winter oceanographic conditions in the fram strait yermak plateau region. *Journal of Geophysical Research*, 97:3469–3483, 1992.

[38] L. Rey. *The Arctic Ocean: The Hydrographic Environment and the Fate of Pollutants*, chapter Water Masses and Energy Exchanges. Wiley-Interscience Publications, 1982.

[39] P.M. Haugan, G.Evensen, J.A. Johannessen, O.M. Johnannessen, and L.H. Pettersson. Modeled and observed mesoscale circulation and wave current refraction during the 1988 norwegian *Geophysical Research*, 96:10487–10506, 1991.

[40] R.Seager, D.S. Battisti, J.Yin, N.Naik, A.C. Clement, and M.A. Cane. Is the gulf stream responsible for europe's mild winters? *Q. J. R. Meteorol. Soc.*, (128):2563–2586, 2002.

[41] T. Martin and R.Gerdes. Sea ice drift variability in arctic ocean model intercomparison project models and observations. *Journal of Geophysical Research*, 112, 2007.

[42] T. Koenigk, U.Mikolajewicz, and H.Haak. Variability of fram strait sea ice export: causes, impacts and feedbacks in a coupled climate model. *Climate Dynamics*, 26:17–34, 2005.

[43] T. Koenigk, U.Mikolajewicz, H.Haak, and J.Jungclaus. *Arctic-Subarctic Ocean Fluxes - Defining the role of the northern seas in climate*, chapter Modelling the Sea Ice Export Through Fram Strait. Springer, 2008.

[44] J. Nilsen, Y. Gao, H. Drange, T. Furevik, and M. Bentsen. Simulated north atlantic- nordic seas water mass exchanges in an isopynic coordinate ogcm. *Geophys. Res. Lett.*, 30, 2003.

[45] J. Zhang, M. Steele, D. Rothrock, and R. Lindsay. Increasing exchanges at greenland-scotland ridge and their links with the north atlantic oscillation and arctic sea ice. *Geophys. Res. Lett.*, 31, 2004.

[46] T.Fichefet and M.A.Morales Maqueda. Sensitivity of a global sea ice model to the treatment of ice thermodynamics and dynamics. *J. Geophys. Res.*, 102:12609–12646, 1997.

[47] B.Bernard, G.Madec, T.Penduff, J.M. Molines, A.M. Treguier, J. LeSommer, A.Beckman, A.Biastoch, C. Boning, J. Dengg, C. Derval, E. Durand, S. Gulev, E. Remy, C. Talandier, S. Theetten, M. Maltrud, J. McClean, and B. DeCuevas. Impact of partial steps amd momentum advectoin schemes in a global ocean ciruclation model at eddy-permitting resolution. *Ocean Dynamics*, 56:543–567, 2006.

[48] *NODC (Levitus) World Ocean Atlas interpolated on ORCA grid NEMO config.*

[49] K.R. Thompson, D.G. Wright, Y. Lu, and E. Demirov. A simple method for reducing seasonal bias and drift in eddy resolving ocean models. *Ocean Model*, pages 122–138, 2006.

[50] J. Stroeve and W. Meier. Sea ice trends and climatologies from smmr and ssm/i. Digital media, National Snow and Ice Data Center, Boulder, CO, 2008. 1978 to 2007.

[51] B.Hansen, S. Osterhus, H.Hatun, R. Kristiansen, and K.M.H. Larsen. The iceland-faroe inflow of atlantic water to the nordic seas. *Progress in Oceanography*, 59:443–474, 2003.

[52] C.W. Boning, M.Scheinert, J.Dengg, A. Biastoch, and A.Funk. Decadal variability of subpolar gyre transport and its reverberation in the north atlantic overturning. *Geophys. Res. Let.*, 33, 2006.

[53] H. Hatun, A. B. Sando, H. Drange, B. Hasen, and H.Valdimarsson. Influence of the atlantic subpolar gyre on the thermohaline circulation. *Science*, 309:1841–1844, 2005.

[54] S. Hakkinen and P.B. Rhines. Decline of the north atlantic subpolar circulation in the 1990s. *Science*, 3(04):555–559, 2004.

[55] I.Polyakov, G.Alekseev, L.Timokhov, U.Bhatt, R.Colony, H.Simmons, D.Walsh, J.Walsh, and V.Zakharov. Variability of the intermediate atlantic water of the arctic ocean over the last 100 years. *Journal of Climate*, 17(23):4485–4497, 2004.

[56] M. Steele and T. Boyd. Retreat of the cold halocline later in the arctic ocean. *J. Geophys. Res.*, 1998.

[57] G. Björk, J. Söderkvist, P. Winsor, A. Nikolopoulos, and M. Steele. Return of the cold halocline layer to the amundsen basin of the arctic ocean: Implications for the sea ice mass balance. *Geophys. Res. Lett.*, 29(11), 2002.

[58] I. Yashayaev. Hydrographic changes in the labrador sea, 1960-2005. *Prog. Oceanogr.*, 73(3-4):242–276, 2007.